Unclassified
JRITY C

NTATION PAGE

Form Approved
OMB No. 0704-0188

AD-A208 657

ELECTE
JUN 06 1989
S D

REPORT
Class

SECURI

1b. RESTRICTIVE MARKINGS

DECLASSIFICATION / DOWNGRADI SCHEDULE

3. DISTRIBUTION / AVAILABILITY OF REPORT
Approved for public release;
Unlimited distribution

(2)

ERFORMING ORGANIZATION REP NUMBER(S)
PC-028-036

5. MONITORING ORGANIZATION REPORT NUMBER(S)
AFOSR-TR- 89-0711

NAME OF PERFORMING ORGANIZATION	6b. OFFICE SYMBOL (If applicable)	7a. NAME OF MONITORING ORGANIZATION
plied Microwave Plasma ncepts, Inc.	AMPC	AFOSR/NP Building 410
ADDRESS (City, State, and ZIP Code)		**7b. ADDRESS (City, State, and ZIP Code)**
75-N Corte Del Nogal rlsbad, CA 92009		Bolling AFB DC 20332-6448
NAME OF FUNDING / SPONSORING ORGANIZATION Air Force Office Scientific Research	**8b. OFFICE SYMBOL (If applicable)** AFOSR/NP	**9. PROCUREMENT INSTRUMENT IDENTIFICATION NUMBER** F49620-86-C-0055
ADDRESS (City, State, and ZIP Code) ilding 410 lling AFB, DC 20332-6448		**10. SOURCE OF FUNDING NUMBERS**

PROGRAM ELEMENT NO.	PROJECT NO.	TASK NO.	WORK UNIT ACCESSION NO.
61102F	2301	A8	

TITLE (Include Security Classification)
ficient Energy Storage and Conversion Using Adiabatic Compression of Relativistic-Electron asmas (Unclassified)

PERSONAL AUTHOR(S)
est, Gareth E., Dandl, Raphael A., and Miller, Robert L.

a. TYPE OF REPORT	13b. TIME COVERED	14. DATE OF REPORT (Year, Month, Day)	15. PAGE COUNT
nal	FROM 86/05/15 TO 88/12/31	89/02/17	34

SUPPLEMENTARY NOTATION

COSATI CODES			18. SUBJECT TERMS (Continue on reverse if necessary and identify by block number)
FIELD	GROUP	SUB-GROUP	

ABSTRACT (Continue on reverse if necessary and identify by block number)

The Plasma Electron Microwave Source
EMS) concept is an approach to producing intense pulses of microwave radiation using energy
ored in a relativistic-electron plasma confined in a magnetic-mirror device. The stored
ergy is transformed into microwaves through amplification of whistler waves that can be
unched externally for amplifier operation or generated spontaneously for oscillator opera-
on. The anisotropy of the hot-electron temperature governs the maximum plasma energy den-
ty that can be stored, the amplification rates, and the saturated power level of the unsta-
e whistler waves. This report summarizes the results of theoretical studies of (1) the
itical aspects of hot-electron plasmas generated by ECH techniques, such as the Upper Off-
sonant Heating pioneered by Dandl in the ELMO series of experiments; and, (2) the spatial
plification rates of unstable whistler waves in these plasmas. It is shown that a substan-
al fraction of the energy stored in a hot-electron plasma can be transformed into repetitive
lses of microwave power by employing the PEMS approach, with typical values of gain, ~ 40db
d bandwidth ~ 1 GHz

. DISTRIBUTION / AVAILABILITY OF ABSTRACT	21. ABSTRACT SECURITY CLASSIFICATION
☒ UNCLASSIFIED/UNLIMITED ☐ SAME AS RPT. ☐ DTIC USERS	Unclassified
. NAME OF RESPONSIBLE INDIVIDUAL Dr. Robert J. Barker	**22b. TELEPHONE (Include Area Code)** (202) 767-4904 / **22c. OFFICE SYMBOL** AFOSR/NP

Form 1473, JUN 86 *Previous editions are obsolete.* SECURITY CLASSIFICATION OF THIS PAGE

89 6 06 079

Unclassified

EFFICIENT ENERGY STORAGE AND CONVERSION USING ADIABATIC COMPRESSION OF RELATIVISTIC-ELECTRON PLASMAS

FINAL REPORT AFOSR-TR- 89-0714

by

G.E. Guest, R.A. Dandl, and R.L.Miller

AMPC, Inc.

February 17, 1989

Work supported by
Air Force Office of Scientific Research
Contract No.
F49620-86-C-0055

NOTICE

TABLE OF CONTENTS

1. INTRODUCTION AND EXECUTIVE SUMMARY

For the period from 15 May 1986 - 15 May 1988, the project described in this report sought to develop a more complete theoretical framework for the Plasma Electron Microwave Source (PEMS) concept (1). The PEMS concept is a novel approach to generating intense pulses of microwave power by transforming energy stored in a mirror-confined hot-electron plasma into large amplitude whistler waves, propagating parallel to the static magnetic field that confines the hot-electron plasma. PEMS devices can function either as amplifiers of externally launched whistler waves or as oscillators, depending on the beta and temperature anisotropy of the hot-electron plasma, where beta is the conventional ratio of plasma kinetic pressure to the magnetostatic pressure of the static magnetic field.

The main objectives of the theoretical research undertaken in this project were to estimate limiting values of the plasma energy that could be stored efficiently in mirror-confined hot-electron plasmas and the fraction of that stored energy that could be transformed into RF field energy. The method of hot-electron plasma generation investigated here is electron cyclotron heating (ECH) including advances such as Upper Off-Resonant Heating(UORH) (2) in which energetic electrons are heated preferentially. Alternative methods for creating the hot-electron plasma using pairs of oppositely-directed co-linear steady-state electron beams are also under active investigation at AMPC. Here our concern is primarily with (1) the limiting values of hot-electron energy density set by instabilities; and (2) the aspects of whistler-wave growth in anisotropic, hot-electron plasmas affecting the gain and output power of PEMS amplifiers and oscillators.

The report consists primarily of two technical sections describing results achieved in each of these two aspects of the problem: Section 2, "Formation of Stable, High-Beta, Relativistic-Electron Plasma Using Electron Cyclotron Heating" [3], has been published recently in Nuclear Fusion. Section 3, "Amplification of Whistler Waves Propagating Through Inhomogeneous, Anisotropic, Mirror-Confined Hot-Electron Plasmas" [4], has been published in Physics of Fluids. The most recent results achieved in this project which have not yet been submitted for publication are reported briefly in Section 4. The remainder of this section provides a recapitulation of the main results using the standard format for final reports.

A one-dimensional, steady state, relativistic Fokker-Planck model of electron cyclotron heating (ECH) is used to analyze heating kinetics underlying the formation of two-component, hot-electron plasmas characteristic of ECH in magnetic mirror configurations. The model is first applied to well diagnosed plasmas studied experimentally in the past and then used to simulate the efficient generation of relativistic-electron plasmas by Upper Off-Resonant Heating (UORH) as has been demonstrated empirically [2]. The characteristics of unstable whistler modes and cyclotron maser modes are then determined numerically for two-component hot-electron plasmas sustained by UORH. Cyclotron maser modes are found to be strongly supressed by cold background-electron species, while whistler growth rates are reduced by relativistic effects to levels that may render them unobservable, provided the hot-electron pressure anisotropy is below an energy-dependent threshold. A fully relativistic local dispersion relation for whistler waves is solved at closely-spaced points along the magnetic

field lines of a 2:1 magnetic mirror in which anisotropic, spatially-inhomogeneous, hot-electron plasmas are confined. The limiting plasma parameters for convective (spatial) growth are determined numerically and used to identify plasma conditions leading to maximum amplification of microwave signals introduced into the plasma in the form of whistler waves. The maximum gain has been evaluated numerically for a range of values of the hot-electron plasma parameters within which all known stability criteria are satisfied. Very high gains (up to 40 dB) are indicated over the range of plasma conditions examined.

1.1 RESEARCH OBJECTIVES OF THE PROJECT:

(1) Obtain self-consistent relativistic-electron distribution functions for optimized electron cyclotron heating using analytical and numerical solution of suitable Fokker-Planck equations.

(2) Test the distribution functions obtained in (1) for violations of equilibrium and/or stability criteria to identify plasma processes limiting the maximum achievable stored energy density.

(3) Determine the effect of spatial inhomogeneities on the propagation and growth of whistlers in the interior of the plasma.

(4) Evaluate the quasi-linear behavior of unstable whistler waves in the interior of plasma.

(5) Model the wave processes governing the reflection, transmission and conversion of whistler waves at the plasma surfaces.

1.2 ACCOMPLISHMENTS AND PROGRESS TOWARD THE OBJECTIVES

(1) Both one- and two-dimensional Fokker-Planck models of relativistic ECH have been solved for a wide range of plasma and magnetic field configurational parameters, including toroidal magnetic geometries as well as simple open-ended magnetic mirrors. Fundamental ECH and Upper Off Resonant Heating results from experiments in ELMO and SM-1 are simulated in all major respects by the Fokker-Planck model.

(2) Equilibrium distributions obtained from the Fokker-Planck models have been analyzed in detail for stability against electromagnetic modes driven by pressure/temperature anisotropy, specifically the so-called "cyclotron maser mode" and unstable whistler waves. In both cases only waves propagating parallel to the static magnetic field have been analyzed, even though the cyclotron maser mode achieves its maximum growth rate for normal propagation. It is found that these modes are completely suppressed by the cold-electron component that is invariably present in ECH plasmas. The whistler wave growth rate is governed by the degree of pressure anisotropy, the hot-electron beta, and the degree to which the hot electrons are affected by the relativistic increase in mass. Highly relativistic hot-electron plasmas are found to exhibit very small whistler growth rates. The condition for existence of equilibria (within the anisotropic guiding center fluid theory) has been evaluated numerically and shown to limit the degree of pressure anisotropy more stringently than the condition for absolutely unstable whistler waves for values of hot-electron beta (perpendicular) greater than 15 - 20%.

(3) A fully relativistic local dispersion relation for whistler waves propagating parallel to the magnetic field has been solved at closely-spaced points along the field lines of a 2:1 magnetic mirror in which anisotropic, spatially inhomogeneous, hot-electron plasma is confined. The limiting plasma parameters for convective (spatial) growth are determined numerically and used to identify plasma conditions leading to maximum overall amplification of microwave signals introduced at one axial edge of the plasma in the form of whistler waves. The maximum gain has been evaluated numerically for a range of values of the hot-electron plasma beta and

temperature anisotropy, within which the major stability criteria are satisfied. Overall (global) gains of 40 dB or more are indicated over the entire range of beta values investigated. Bandwidths in excess of 15 - 20% are obtained at low beta; and much larger bandwidths are found in the more relativistic cases with higher betas.

(4) In anticipation of rather sophisticated numerical studies of the nonlinear evolution of spatially growing whistler waves, almost certainly requiring numerical simulation techniques, we have carried out preliminary estimates of the maximum energy that can be transformed into wave energy using thermodynamic bounds developed by T.K. Fowler (5). Fowler defined a type of free energy that is appropriate for plasmas capable of sustaining microturbulent phenomena, such as the growth of high-frequency waves. The magnitude of the free energy, together with the dynamical constraints associated with the Vlasov kinetic equation leads to a bound on the maximum amplitude of the unstable waves. In the present case, Fowler's estimate for the limiting amplitude of the RF electric field energy is directly proportional to the hot-electron plasma energy and the degree of temperature anisotropy relative to a marginally stable case. The estimated fraction of the hot-electron stored energy that can be transformed into wave energy for the cases examined to date can range up to 50%.

(5) We have identified a promising spatially varying plasma configuration that offers the possibility of minimal internal reflection of whistler waves launched at one end of the plasma. The hot-electron plasma is confined in a 2:1 magnetic mirror with an arbitrarily long flat field central region. The effective axial boundaries of the hot-electron plasma are taken to be the fundamental ECH resonant surfaces; within this central region cold plasma is generated uniformly through ionization of incident neutral gas. The cold plasma flows freely along the lines of force and expands in the region beyond the magnetic mirrors, where the magnetic lines of force diverge. Since the propagation velocity of whistler waves approaches the speed of light as the plasma density decreases by virtue of the diverging magnetic field lines, we anticipate efficient coupling to outgoing vacuum electromagnetic waves.

SECTION 2

FORMATION OF STABLE, HIGH-BETA, RELATIVISTIC-ELECTRON PLASMAS USING ELECTRON CYCLOTRON HEATING

G.E. GUEST, R.L. MILLER
Applied Microwave Plasma Concepts, Inc.,
Carlsbad, California,
United States of America

ABSTRACT. A one-dimensional, steady-state, relativistic Fokker-Planck model of electron cyclotron heating (ECH) is used to analyse the heating kinetics underlying the formation of the two-component hot-electron plasmas characteristic of ECH in magnetic mirror configurations. The model is first applied to the well diagnosed plasmas obtained in SM-1 and is then used to simulate the effective generation of relativistic electrons by upper off-resonant heating (UORH), as demonstrated empirically in ELMO. The characteristics of unstable whistler modes and cyclotron maser modes are then determined for two-component hot-electron plasmas sustained by UORH. Cyclotron maser modes are shown to be strongly suppressed by the colder background electron species, while the growth rates of whistler modes are reduced by relativistic effects to levels that may render them unobservable, provided the hot-electron pressure anisotropy is below an energy dependent threshold.

1. INTRODUCTION

Early experiments on electron cyclotron heating (ECH) of plasmas confined in magnetic mirrors [1] using CW microwave power at a single frequency created an unusual plasma containing two distinct populations of electrons. The majority of the electrons remained at a temperature that was typically below 100 eV, while a small fraction was heated to average energies above 100 keV. Rather broad regimes of stable operation were found to be limited by the onset of several dominant modes of instability, such as the mirror mode, the flute mode and unstable whistler waves. Later experiments in the ELMO facility [2] showed that the energy stored in the hot-electron component could be greatly increased by using upper off-resonant heating (UORH), in which microwave power at a frequency above the cold-electron gyrofrequency was added to the fundamental ECH power. In addition to increasing the relative density of the hot electrons, UORH also enhanced the stability of the plasma, even for values of beta in excess of 50% (beta is the conventional ratio of plasma kinetic pressure to magnetostatic pressure).

The stable, high-beta, hot-electron annulus revealed by the ELMO experiments led to the successful use of these plasmas ('ELMO rings') to stabilize a scalar pressure core plasma confined in the ELMO Bumpy Torus device (see, for example, Ref. [3]); this stimulated widespread interest in the fundamental properties of these remarkable plasmas (see, for example, Ref. [4]). Recently proposed applications for these hot-electron plasmas include stabilization of localized modes in heliacs [5] and tokamaks [6], as well as energy storage for subsequent conversion to high-power microwave pulses.

It has required the efforts of many workers to evolve reasonably satisfactory theoretical models of the steady state equilibrium produced in ECH experiments. The basic characteristics of the interaction of individual electrons with microwave electric fields were derived very early (for a discussion of early theoretical work, see Ref. [7]) and useful formulas were obtained for the resulting heating rate under a wide range of conditions (for a description of later work, see Ref. [8]). Subsequent development of geometrical optics codes (see, for example, Ref. [9]) made it possible to describe the propagation and absorption of microwaves in specified plasma media. Progress was accelerated by the formulation of a relativistic Fokker-Planck theory of ECH by Bernstein and Baxter [10]. Hamasaki and co-workers [11] took moments of the Fokker-Planck equation, using trial distribution functions, in an attempt to predict the power required for formation of the ELMO rings. Other workers [12] developed numerical techniques for a direct solution of the Fokker-Planck

equation; these are now implemented in large computer codes [13]. Ultimately, these codes are expected to provide a detailed, self-consistent picture of high-beta hot-electron plasmas formed by ECH.

Nonetheless, there is an immediate need for a reduced model that can be used to search over the wide range of parameters characterizing an ECH experiment. It is not practical to carry out such a search with two-dimensional Fokker-Planck codes; this would require broad, time consuming parameter searches to overcome the general lack of experimental measurements of such essential parameters as the strength of each RF electric field component present in the plasma. We have addressed this need by evolving a Fokker-Planck model for the steady state distribution of electrons in energy; this model includes in a heuristic way the phenomena that depend essentially on the electron orientation in a gyrotropic, two-dimensional velocity space. This model has been described in considerable detail in Ref. [14].

In order to model a complex physical situation in a relatively simple way, the power balance issues affecting the formation of a relativistic electron tail have been considered primarily and not the particle balance issues, except in so far as a significant associated energy loss occurs, as in the case of non-adiabatic scattering of high energy electrons into the loss cone. For a more detailed justification of this approach, see the Appendix. Thus, we have chosen to conserve particles while accounting for the energy loss by converting the non-adiabatic loss term into a dynamical friction term, as described in Appendix C of Ref. [14]. This choice has the desired physical effect of sharply reducing the hot-electron distribution function for energies above the threshold for violation of adiabatic invariance, as is clearly evident in Figs 1a and 1b. The hot-electron distribution in energy is shown in Fig. 1a for plasmas typical of those reported in Ref. [15]. Figure 1b shows the four rates accounted for in the model: the quasi-linear heating rate, the Coulomb thermalization rate, the synchrotron radiation cooling rate and the energy loss rate due to non-adiabatic scattering.

Here, we first apply this reduced model to the SM-1 experiments [15] in order to demonstrate the success of this model in describing the hot-electron plasmas studied in SM-1. The results of this demonstration are presented and discussed in Section 2. They clarify a number of features of ECH experiments that had not been fully understood previously. In particular, the role of microwave electric fields parallel to the static magnetic field (ordinary mode of propagation) is

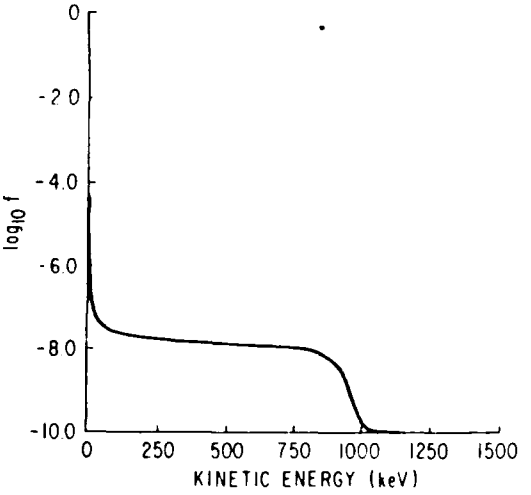

FIG. 1a. Electron distribution in energy for a case typical of the single-frequency heating experiments reported in Ref. [15].

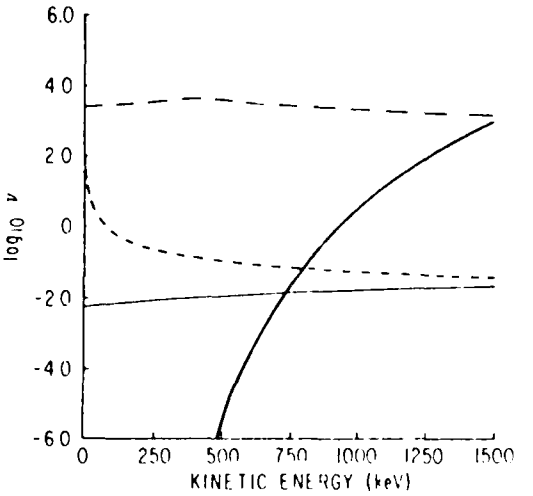

FIG. 1b. Characteristic rates entering into the heating kinetics (from top): electron heating rate due to ECH power, electron thermalization by Coulomb collisions with colder electrons, synchrotron radiation, and energy loss by non-adiabatic scattering of hot electrons into the loss cone.

shown to be critical to an effective formation of the hot-electron component. Furthermore, by exploiting the sensitivity of the hot-electron heating rate to the parallel microwave electric fields, we are able to use the reduced Fokker-Planck ECH model to demonstrate the impact of non-adiabatic scattering [16], which has been conjectured for some time to limit the maximum temperature of the hot electrons in most ECH experiments to date.

We then apply the present model to the UORH experiments in ELMO [2], where the model displays the same striking increases in stored energy with increasing UORH power that were observed in ELMO. Finally, the model is used to obtain high-beta hot-electron equilibria suitable for subsequent stability studies. Although the reduced model cannot provide information on pressure anisotropies or other two-dimensional properties of the equilibria, it does relate the relative temperatures and densities of the two electron species and provides a much larger degree of internal consistency than was heretofore available.

In Section 3, we analyse the stability of the hot-electron plasmas to transverse waves propagating along the static magnetic field, namely whistler waves [17] and the cyclotron maser modes (see, for example, Ref. [18a] and the excellent set of references cited therein; for more recent results, see Ref. [18b]). It has been known for many years [19] that relativistic effects generally reduce the growth rates of unstable whistler waves, but specific results depend on the assumed equilibrium. Here we use the Fokker-Planck model to obtain equilibria that are consistent with ECH kinetics and demonstrate the relativistic suppression of whistler growth rates. The cyclotron maser modes are found to be completely stabilized by the cold-electron component.

Finally, we note in passing that our understanding of flute modes in high-beta hot-electron plasmas has not been considered here and remains incomplete, although fully electromagnetic kinetic models of line tying [20] have helped clarify finite-length effects. There is an active effort to predict the stability of these high-beta plasmas to flute-like modes [21] which we hope will be aided by more detailed descriptions of realistic equilibria. Discussion and conclusions are found in Section 4.

2. FORMATION OF HOT-ELECTRON PLASMAS USING ECH

In this section we describe the results of applying the reduced Fokker-Planck ECH model to ECH experiments in the mirror devices SM-1 [15] and ELMO [2] before using the model to obtain high-beta equilibria for stability analysis. The Fokker-Planck model is described in great detail in Ref. [14] and references cited there.

Briefly, we use a one-dimensional, steady-state, bounce-averaged Fokker-Planck model of the ECH process. Since our primary concern is with the thermalization of a relatively small concentration of energetic electrons, we adopt a linearized, test particle framework. The relativistic ('hot') electrons are then regarded as a distinct species whose spatial density n_h is much smaller than the densities of the other plasma species. All of these 'field' species are assumed to be isotropic, thermal, and at a much lower temperature than the hot electrons. This model determines the response of a small relative-density, high-energy electron tail to the incident microwave power by including the dominant dynamical processes: quasi-linear heating, thermalization by Coulomb scattering on cooler electrons, synchrotron radiation, and direct loss by non-adiabatic scattering. Specifically, the model predicts the electron distribution in energy resulting from RF electric fields with specified values of frequency, amplitude and polarization, incident upon a background plasma of specified density and temperature, confined in a prescribed mirror-like magnetic field.

TABLE I. SM-1 REFERENCE CASE (Ref. [15])

Stored energy	$W = 20$ J
Radius of annulus	$r_0 = 10.4$ cm
Radial width	$2\Delta = 5.8$ cm
Axial length	$L/2 = 12$ and 18 cm
Annulus volume	$Vol = 12 \times 10^3$ cm^3
Mirror ratio on axis	$M_0 = 2.2$
Coil separation	$L_c = 71$ cm
Mirror ratio at r_0	$M = 3$
Mirror ratio at resonance	$M_{res} = 2$
ECH power	$P \approx 1$ kW
Microwave frequency	$f \approx 9.5$ GHz
Background plasma	
density	$n \approx (1\text{-}3) \times 10^{11}$ cm^{-3}
temperature	$T_c \approx 10\text{-}50$ eV
Hot-electron component	
density	$n_h \approx 3 \times 10^{10}$ cm^{-3}
temperature	$T_h \approx 350\text{-}400$ keV

We take as our SM-1 reference case the 20 J equilibrium discussed at length in Ref. [15] and summarized in Table I. As mentioned earlier, there are no direct measurements of the strength of the microwave electric fields, and we must scan over all plausible values of both components, E_- and E_+. We do this by specifying the ratio E_+/E_- of the O-mode and X-mode field strengths and searching out the values of

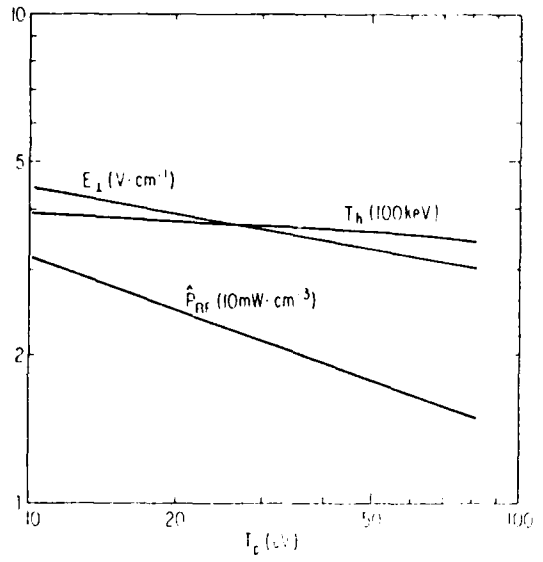

FIG. 2a. Perpendicular component of the microwave electric field, $E_\perp$, average energy of the hot electrons, T_h, and total RF power density, $\hat{P}_{Rf}$, versus background plasma temperature, T_e, for an assumed ratio of O-mode to X-mode field strengths, $E_\parallel/E_\perp = 2$, in the SM-1 configuration summarized in Table I. The relative hot-electron density is $n_h/n = 0.1$.

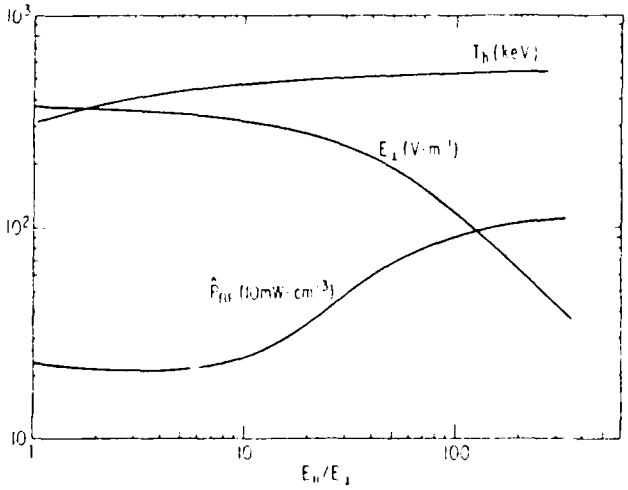

FIG. 2b. Variation of $E_\perp$, T_h and RF power density $\hat{P}_{Rf}$ with $E_\parallel/E_\perp$ for a background plasma temperature $T_e = 30$ eV and $n_h/n = 0.1$

$E_\perp$ required to sustain the observed relative hot-electron density, $n_h/n = 0.1$; this yields the observed hot-electron average energy T_h and the RF power density $\hat{P}_{Rf}$ required to sustain the equilibrium. Since the microwave power is launched primarily in ordinary modes and is multiply reflected from the cavity walls, we assume an essentially isotropic distribution of wave vectors $\vec{k}$ for the ECH waves. An illustrative case is shown in Fig. 2a, which displays $E_\perp$, T_h and $\hat{P}_{Rf}$ versus the background electron temperature T_e for $E_\parallel/E_\perp = 2$. The characteristic scale length of the static magnetic field has been set at $L_r = 30$ cm for this case, a choice that we will discuss at length in the following. Note that the RF power density required to sustain this equilibrium is around 20 mW·cm^{-3}, accounting for roughly 250 W of RF power. This does not include the fundamental ECH power necessary to sustain the background plasma. If the energy expended in creating each ion-electron pair is roughly 50 eV, we estimate this fundamental ECH power requirement at 25 mW·cm^{-3} for an ambient hydrogen gas pressure of 5×10^{-6} torr. Since the cold-plasma volume is estimated at 25 L in Ref. [15], as much as 625 W of fundamental ECH power may be required simply to sustain the background plasma and only 250 W may be required to sustain the hot-electron component. The variation of $E_\perp$, T_h and $\hat{P}_{RF}$ with the ratio $E_\parallel/E_\perp$ is shown in Fig. 2b for a background electron temperature $T_e = 30$ eV. Note the rapid rise in RF power density for $E_\parallel/E_\perp > 10$, in which $\hat{P}_{RF}$ increases five times while the average energy of the hot electrons remains almost constant. The saturation of T_h despite a substantial increase in RF power indicates the rapid increase in the non-adiabatic scattering rate. If these calculations are repeated for different values of the magnetic scale length L_r, we obtain the striking results shown in Fig. 3a. It is especially instructive to display the L_r dependence of the saturated value of the hot-electron average energy and the corresponding values of the electron gyroradius:

$$\rho_{cyl} = 1.7 \times 10^3 \text{ G·cm} \sqrt{\epsilon(2 + \epsilon)}/B$$

where $\epsilon = T_{h\,sat}/m_0c^2$ and B is the magnetic intensity. Since we require $\rho \leq kL_r$ for adiabatic confinement of electrons, we can evaluate k by plotting ρ_{cyl} versus L_r. The value of k obtained from Fig. 3b is 0.06, which agrees reasonably well with the conventional result cited by Uckan [16]. From the values obtained for $T_{h\,sat}$ it appears that $L_r = 24$ cm is a reasonable value of the magnetic scale length in the hot-electron region of SM-1. From a parabolic fit to the vacuum magnetic intensity we would estimate $L_r = 21$ cm, in reasonable agreement. Note that this is much less than R_c, the radius of curvature of the magnetic field lines in this region, which is estimated to be around 60 cm.

For large values of L_r, particularly at higher magnetic fields, synchrotron radiation becomes a dominant loss mechanism in the model. This loss is

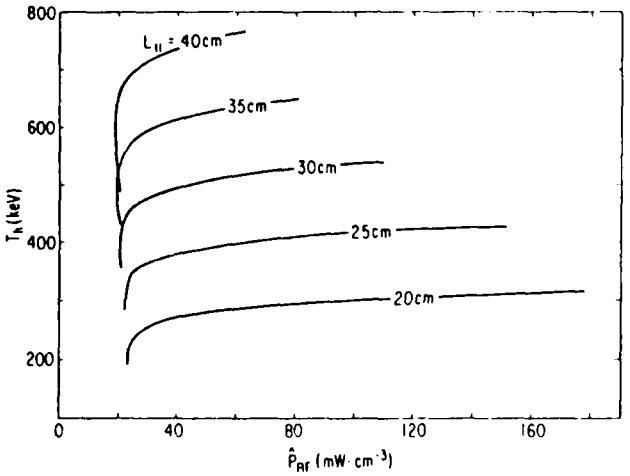

FIG. 3a. T_h versus $\hat{P}_{RF}$ for different values of the magnetic scale length $L_{||}$.

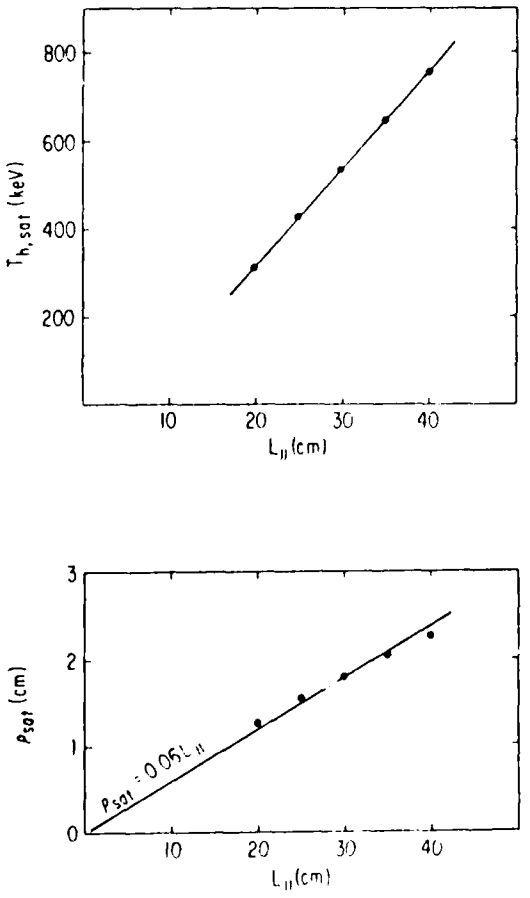

FIG. 3b. Saturated value of $T_{h,sat}$ and corresponding value of the average hot-electron gyroradius ρ_{sat} versus $L_{||}$. The solid line is for $\rho_{sat} = 0.06\, L_{||}$.

circumvented in the case discussed here by specifying values of $L_{||}$ similar to the ELMO (high field) experiments: $L_{||}$ = 10 cm (ELMO).

Another important feature of the dependence of T_h on $E_{||}/E_{\perp}$ is the rapid initial increse in T_h, with $\hat{P}_{RF}$ constant or even decreasing. This behaviour makes clear the substantial benefit of increased microwave integrity of the vacuum chamber. If $E_{||}/E_{\perp} \geq 10$ can be sustained in a suitably designed cavity where wall reflections do not rapidly convert ordinary modes to extraordinary modes, T_h can be increased by roughly 100 keV or more. Since the value of $E_{||}$ required to achieve this level of heating is approximately 10^2 V·cm^{-1}, while the power density dissipated in the plasma is around 1 W·cm^{-3}, the effective quality factor must exceed 300. The ELMO device [2] utilized a very high-Q cavity together with UORH power to obtain exceptionally efficient heating of relativistic electrons. The frequency of the UORH power is chosen to be above the cold electron gyrofrequency throughout the entire cavity. This power is therefore absorbed primarily by the relativistic electrons and only negligibly by the background electrons. Even for the hot electrons, the absorption rate is small; thus, if the cavity has a large quality factor, the electric field strength can increase to large enough values to render the heating rate (and hence the absorption rate) appreciable. Since heating rates are quadratic in electric field strength, they can be large enough to sustain high energy electron populations at levels below 100 V·cm^{-1}.

The Fokker-Planck simulation of early ELMO experiments on UORH [2] are shown in Fig. 4. Here the fundamental ECH is at a frequency of 10.6 GHz while the UORH source has a frequency of 35.7 GHz. These results compare favourably with the empirical results displayed in Fig. 4 of Ref. [2]. The background plasma density and temperature are 2×10^{11} cm^{-3} and 50 eV, respectively, and we have arbitrarily set $E_{||}/E_{\perp} = 10$ for both sources. In the absence of UORH power, the relative density of hot electrons is roughly 2.5%, sustained by an RF power density of less than 6 mW·cm^{-3}. This relative density increases to 64% and the hot-electron beta approaches 50% as the UORH power is increased.

Having calibrated our model on SM-1 and ELMO, it is of interest to see how much hot-electron energy can be stored in comparably sized devices by optimizing the parameters. By using UORH at higher frequencies (60/90 GHz) in a device that is similar in physical scale to ELMO, we can obtain Fokker-Planck equilibria with average hot-electron energies above

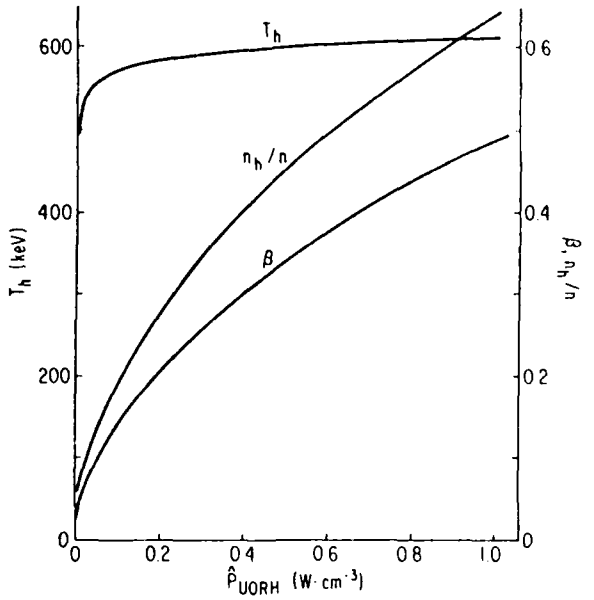

FIG. 4. Average hot-electron energy, T_h, relative hot-electron density, n_h/n, and plasma beta, β, versus power density from the UORH source, $\hat{P}_{UORH}$. The parameters describing the background plasma and the heating configuration are given in the text.

m_0c^2. The relativistic effects on plasma stability can be clearly examined in this hot-electron temperature range. In these studies, we have again specified the background plasma density at $n = 1 \times 10^{13}$ cm^{-3} and varied the background electron temperature T_c from 250 to 3000 eV. We assume that optimal background electron temperatures can be maintained by a suitable level of fundamental ECH power, depending mainly on the confinement properties of the configuration. For the Fokker–Planck model of the hot-electron population we reduce the fundamental ECH electric field strength to a negligible level: 10^{-3} times the UORH field strength. We then vary T_c over its range to determine the values of UORH power density $\hat{P}_{RF}$ required to sustain specified relative densities of hot electrons. The Fokker–Planck model evaluates T_h for specified values of the various system parameters, such as the magnetic field scale length L_f, here set at 10 cm, as in ELMO. These results are displayed in Fig. 5. Note that, since these curves are deduced for constant hot-electron densities $\Delta_h = n_h/n$, the resulting value of beta is simply porportional to T_h. The RF power density exhibits a broad minimum that moves from 500 eV to 800 eV as the hot-electron density ratio is increased from 10% to 40%. The associated beta values approach 50% and the hot-electron average energy is around 550 keV. These are the equilibria whose stability will be studied in the following sections.

3. STABILITY ANALYSIS FOR TRANSVERSE WAVES PROPAGATING PARALLEL TO THE STATIC MAGNETIC FIELD

As discussed in Section 2, the first task addressed in this work was to obtain high-beta equilibria from the reduced one-dimensional Fokker–Planck model of the ECH process. Guided by the empirical results of Dandl et al. [2] on UORH in the ELMO experiments, we found a corresponding regime in the Fokker–Planck analysis that yields high-beta, relativistic-electron equilibria ideally suited to a stability analysis, namely beta values around 50% and relativistic-electron temperatures above 500 keV. Our one-dimensional Fokker–Planck model cannot provide any information on the temperature anisotropy that is characteristic of hot-electron plasmas formed by ECH and which plays a dominant role in the stability of these plasmas [22]. Fully two-dimensional Fokker–Planck ECH codes are now available and will eventually provide two-dimensional equilibria. These numerical equilibria can be expressed analytically as a superposition of the equilibrium distribution functions described by Guest and Dory [23]:

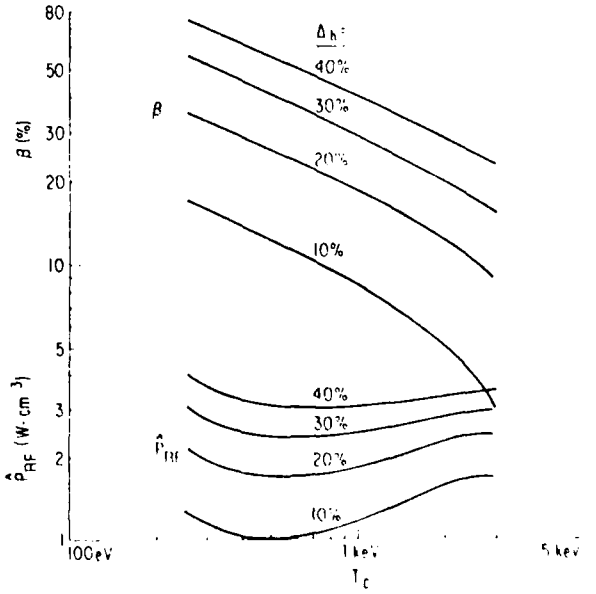

FIG. 5. RF power density required and beta value achieved in maintaining specified values of relative hot-electron density versus background electron temperature T_c. The background plasma density is 10^{13} cm^{-3} and the ECH frequencies are 60 and 90 GHz.

$$f^{(0)}(u_\perp^2, u_\parallel^2) = \frac{n}{\pi^{3/2}\alpha_\perp^2\alpha_\parallel \ell!}\left[\frac{u_\perp}{\alpha_\perp}\right]^{2\ell} \times \exp\left[-\frac{u_\perp^2}{\alpha_\perp^2} - \frac{u_\parallel^2}{\alpha_\parallel^2}\right]$$

where $\ell = 0, 1, 2, \ldots$, and $\vec{u} = \vec{p}/m$ is the momentum per unit rest mass. Here, we examine our one-dimensional equilibria for stability against transverse waves propagating parallel to the static magnetic field, with the temperature anisotropy $\eta \equiv T_\perp/T_\parallel$ and the loss-cone index ℓ set at arbitrary values. We single out the whistler mode [17, 19, 24] and the cyclotron maser mode [18, 24] because of the relative stringency of the stability criteria for electrostatic and whistler modes, as discussed by Guest and Sigmar [22], and because the cyclotron maser mode was omitted from consideration in Ref. [22].

In what follows, we describe an efficient and very rapid numerical technique for solving the fully relativistic dispersion relation for right-hand, circularly polarized, transverse waves propagating parallel to the equilibrium magnetic field. The derivation of the dispersion relation is sketched here for completeness; more detailed discussions are readily available [25].

The relativistic Vlasov equation for electrons is

$$(\partial f/\partial t) + (\vec{u}/\gamma)(\partial f/\partial \vec{r}) - (e/m)[\vec{E} + (\vec{u} \times \vec{B})/\gamma](\partial f/\partial \vec{u}) = 0$$

where $\gamma^2 = 1 + u^2/c^2$ is the Lorentz factor and the velocity is $\vec{v} = \vec{u}/\gamma$. The perturbed distribution function, associated with a wave whose electric and magnetic fields are $\vec{E}$ and $\vec{B} = \vec{k} \times \vec{E}/\omega$, is given by

$$f_1(\vec{r}, \vec{u}, t) = \frac{e}{m}\int_{-\infty}^{t} dt' \times \left[\left(1 - \frac{\vec{k}\cdot\vec{u}}{\gamma\omega}\right)\vec{E}\cdot\frac{\partial f_0}{\partial \vec{u}} + \frac{\vec{u}\cdot\vec{E}}{\gamma\omega}\vec{k}\cdot\frac{\partial f_0}{\partial \vec{u}}\right]$$

For purely transverse waves propagating parallel to the equilibrium magnetic field, with components $E_\pm = (E_x \pm iE_y)/\sqrt{2}$, this expression becomes

$$f_1(\vec{r}, \vec{u}, t) = \sqrt{2}\,\frac{e}{m}\int_{-\infty}^{t} dt' \times \left[\left(1 - \frac{ku_\parallel}{\gamma\omega}\right)\frac{\partial f_0}{\partial u_\perp^2} + \frac{ku_\parallel}{\gamma\omega}\frac{\partial f_0}{\partial u_\parallel^2}\right] \times u_\perp(E_+ e^{-i\phi} + E_- e^{i\phi})$$

where ϕ is the polar angle. In the uniform magnetic field assumed here, the unperturbed electron orbits are given by $z = z_0 + u_\parallel t/\gamma$ and $\phi = \phi_0 + eBt/\gamma m$, with $u_\parallel$ and $u_\perp$ constant. Choosing $z_0 = 0$ at $t = 0$, we obtain

$$f_1(z=0, \vec{u}, t=0) = -i\sqrt{2}u_\perp(e/m) \times \left[\left(\gamma - \frac{ku_\parallel}{\omega}\right)\frac{\partial f_0}{\partial u_\perp^2} + \frac{ku_\parallel}{\omega}\frac{\partial f_0}{\partial u_\parallel^2}\right] \times \left(\frac{E_+ e^{i\phi}}{ku_\parallel - \gamma\omega - eB/m} + \frac{E_- e^{i\phi}}{ku_\parallel - \gamma\omega + eB/m}\right)$$

From Faraday's and Ampere's laws,

$$\nabla \times (\nabla \times \vec{E}) = -\mu_0(\partial/\partial t)[\vec{j} + \epsilon_0(\partial\vec{E}/\partial t)]$$

or

$$k^2\vec{E} - (\vec{k}\cdot\vec{E})\vec{k} - (\omega^2/c^2)\vec{E} = i\omega\mu_0\vec{j}$$

Since $\vec{k}\cdot\vec{E} = 0$ for transverse waves, $\vec{E}$ and $\vec{j}$ must satisfy

$$[(k^2c^2/\omega^2) - 1]\vec{E} = (i/\omega\epsilon_0)\vec{j}$$

For the right-hand, circularly polarized component, the resulting dispersion relation is

$$\frac{k^2c^2}{\omega^2} - 1 = \frac{-e^2}{m\omega\epsilon_0}\,2\pi\int_0^\infty u_\perp^2\,du_\perp\int_{-\infty}^{\infty} du_\parallel \times \frac{\left(1 - \frac{ku_\parallel}{\gamma\omega}\right)\frac{\partial f_0}{\partial u_\perp^2} + \frac{ku_\parallel}{\gamma\omega}\frac{\partial f_0}{\partial u_\parallel^2}}{ku_\parallel - \gamma\omega + eB/m}$$

For the class of equilibrium distribution functions discussed by Guest and Dory [23], the numerator of the integrand can be rewritten conveniently as

$$\left(1 - \frac{ku_\parallel}{\gamma\omega}\right)\frac{\partial f_0}{\partial u_\perp^2} + \frac{ku_\parallel}{\gamma\omega}\frac{\partial f_0}{\partial u_\parallel^2}$$

$$= \frac{f_0}{\alpha_\perp^2}\left[\frac{ku_\parallel}{\gamma\omega}\left(1 - \frac{\ell\alpha_\perp^2}{u_\perp^2} - \frac{\alpha_\perp^2}{\alpha_\parallel^2}\right) - \left(1 - \frac{\ell\alpha_\perp^2}{u_\perp^2}\right)\right]$$

Since the Lorentz factor γ appears in the resonant denominator and since we are concerned with strongly relativistic plasmas with $\gamma \gtrsim 2$, it is necessary to evaluate the integral numerically. We now consider integrals of the general form

$$I(\omega, k) = \int_0^\infty du_\perp^2\, e^{-u_\perp^2/\alpha_\perp^2} \int_{-\infty}^\infty du_\parallel\, e^{-u_\parallel^2/\alpha_\parallel^2} \times \frac{F(u_\parallel, u_\perp^2, \omega, k)}{ku_\parallel - \gamma\omega + eB/m}$$

For complex values of ω and k, there may be zero, one or two solutions to the relativistic resonance condition $ku_\parallel - \gamma\omega + eB/m$, which we denote by $u_{\parallel i}$ $(i = 1, 2)$. We denote each solution for $u_\parallel(\omega, k, u_\perp^2)$ by w and the corresponding values of γ by $\gamma_i^2 = \sqrt{1 + w_i^2/c^2 + u_\perp^2/c^2}$. Now consider the following integral:

$$\int_{-\infty}^\infty du_\parallel\, e^{-u_\parallel^2/\alpha_\parallel^2} \frac{F(w_i, u_\perp^2, \omega, k)}{ku_\parallel - \gamma_i\omega + eB/m}$$

$$= \alpha_\parallel F(w_i, u_\perp^2, \omega, k) \int_{-\infty}^\infty dy \frac{e^{-y^2}}{k\alpha_\parallel y - \gamma_i\omega + eB/m}$$

$$= \frac{\sqrt{\pi}}{k} Z\left(\frac{\gamma_i\omega - eB/m}{k\alpha_\parallel}\right) F(w_i, u_\perp^2, \omega, k)$$

for $\quad \mathrm{Im}\left(\frac{\gamma_i\omega - eB/m}{k\alpha_\parallel}\right) > 0$

where Z is the conventional plasma dispersion function [26]. From this, we obtain:

$$I(\omega, k) = \int_0^\infty du_\perp^2\, e^{u_\perp^2/\alpha_\perp^2} \frac{\sqrt{\pi}}{k} Z\left(\frac{\gamma_i\omega - eB/m}{k\alpha_\parallel}\right) \times F(w_i, u_\perp^2, \omega, k) + \int_0^\infty du_\perp^2\, e^{-u_\perp^2/\alpha_\perp^2} \int_{-\infty}^\infty du_\parallel\, e^{-u_\parallel^2/\alpha_\parallel^2} \times \left(\frac{F(u_\parallel, u_\perp^2, \omega, k)}{ku_\parallel - \gamma\omega + eB/m} - \frac{F(w_i, u_\perp^2, \omega, k)}{ku_\parallel - \gamma_i\omega + eB/m}\right)$$

With the singularities removed in this manner, the $u_\parallel$ integral can be evaluated using the Gauss-Hermite quadrature [27]:

$$\int_{-\infty}^\infty du_\parallel\, e^{-u_\parallel^2/\alpha_\parallel^2} \Xi(u_\parallel) = \sum_{i=1}^s W_{H,i}\, \Xi(u_{\parallel,i})$$

Similarly, the $u_\perp$ integral can be evaluated using the Gauss-Laguerre quadrature [26]

$$\int_0^\infty du_\perp^2\, e^{-u_\perp^2/\alpha_\perp^2} \Psi(u_\perp^2) = \sum_{i=1}^s W_{L,i} \Psi(u_{\perp,i}^2)$$

To evaluate the dispersion relation for given values of ω and k, we then choose a value of s ($s = 12$ typically) and for each of the s prescribed values of $u_{\perp,i}^2$ $(i = 1, \ldots, s)$ we evaluate the corresponding root or roots of the relativistic resonance condition, $u_{\parallel,i} = w_i$, such that

$$k_\parallel w_i - \hat{\gamma}_i\omega_r + eB/m = 0$$

The Gauss-Hermite formula is then used to calculate

$$G(\omega, k, u_{\perp,i}^2) \equiv \int_{-\infty}^\infty du_\parallel\, e^{-u_\parallel^2/\alpha_\parallel^2} \times \left(\frac{F(u_\parallel, u_{\perp,i}^2, \omega, k)}{ku_\parallel - \omega\sqrt{(1 + (u_\parallel^2/c^2) + (u_{\perp,i}^2/c^2))} + eB/m} - \frac{F(w_i, u_{\perp,i}^2, \omega, k)}{ku_\parallel - \omega\sqrt{(1 + (w_i^2/c^2) + (u_{\perp,i}^2/c^2))} + eB/m}\right)$$

$$= \sum_{i=1}^s W_{H,i}\, \Xi_i(u_{\parallel,i}, u_{\perp,i}^2, \omega, k)$$

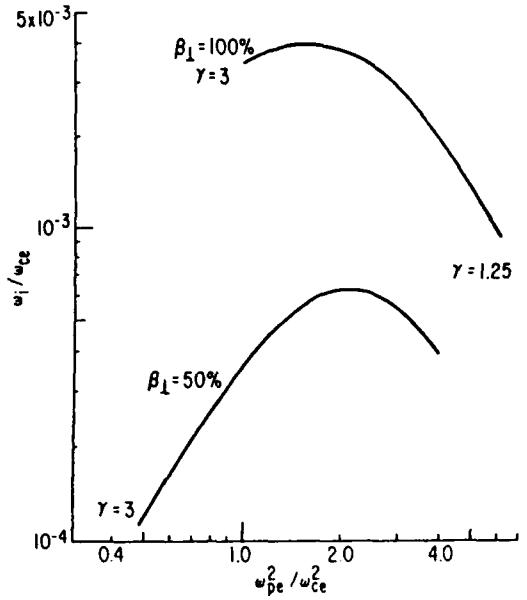

FIG. 6. Density dependence of cyclotron maser mode growth rate for fixed values of beta. The plasma parameters are specified in the text.

A standard routine is used to evaluate the plasma dispersion function, and the Gauss-Laguerre quadrature is used to evaluate the $u_\perp^2$ integral:

$$I(\omega, k) = \int_0^\infty du_\perp^2 \, e^{-u_\perp^2/\alpha^2}$$

$$\times \left[\frac{\sqrt{\pi}}{k} Z\left(\frac{\hat{\gamma}\omega - eB/m}{k\alpha_\parallel} \right) F(w_i, u_\perp^2, \omega, k) \right.$$

$$\left. + G(\omega, k, u_\perp^2) \right] = \sum_{p=1}^{s} W_{L,p} \, \Xi_2(u_{\perp,p}^2, \omega, k)$$

With this algorithm for evaluating the velocity-space integrals, we can use standard root-finding routines to solve the dispersion relation for fully relativistic hot-electron plasmas. In this way we can evaluate the threshold conditions and growth rates for unstable whistler and cyclotron maser modes in the high-beta hot-electron plasmas obtained from our Fokker-Planck model. As has been pointed out by Chu and Hirshfield [18a], whistler waves with phase velocities below the speed of light are destabilized by the temperature anisotropy, while the cyclotron maser mode, corresponding to waves with phase velocities greater than the speed of light, are destabilized by the beam-like/loss-cone aspect of the mirror-confined relativistic-electron equilibria [28]. Of particular interest for the present studies is the stabilizing effect of a cold-electron component on the cyclotron maser mode. Since our Fokker-Planck ECH equilibria consist of a minority population of relativistic electrons in a majority population of much colder background electrons, cyclotron maser modes are anticipated to be strongly suppressed. This is illustrated in the results shown in Fig. 6, where we fix the beta value at 50% and 100%, and the relative density of hot electrons at 30%. The hot-electron distribution has a loss cone index $\ell = 2$, and a temperature anisotropy $\eta \equiv T_\perp/T_\parallel = 3$. The peak temporal growth rate ω_i normalized by the (non-relativistic) electron gyrofrequency ω_{ce} is plotted against the total electron density, specified through the ratio of electron plasma and gyrofrequencies, $(\omega_{pe}/\omega_{ce})^2$. For the parameters of interest, the peak growth rates are less than 10^{-3} times the gyrofrequency. Figures 7a and 7b demonstrate the fundamental dependence of the cyclotron maser modes on the loss-cone index ℓ, rather than the temperature anisotropy. For these cases, the hot-electron beta is fixed at 30%, the total density at $\omega_{pe}^2 = \omega_{ce}^2/2$, and the relative density of hot electrons at 50%.

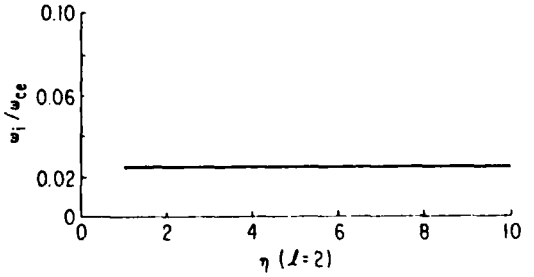

FIG. 7a. Demonstration of the independence of the cyclotron maser mode growth rate with respect to temperature anisotropy.

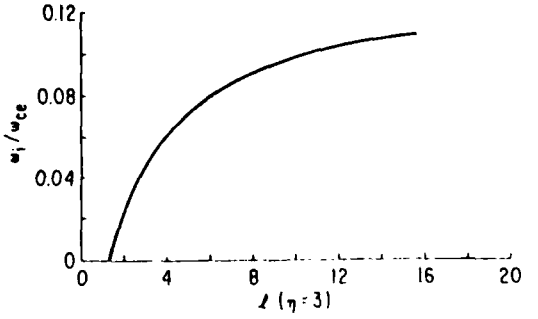

FIG. 7b. Dependence of the cyclotron maser mode growth rate on the loss-cone index ℓ.

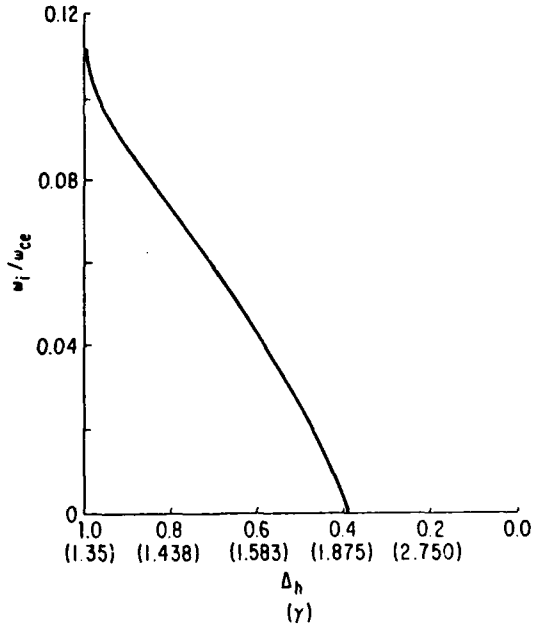

FIG. 8. Stabilization of the cyclotron maser mode by background cold electrons. The relative density of hot electrons is $\Delta_h = n_h/n$.

Finally, Fig. 8 shows how the growth is suppressed by decreasing the relative density of hot electrons, Δ_h. In this particular case, stabilization is complete for $\Delta_h \lesssim 40\%$; here, $\beta = 30\%$ and $\omega_{pe}^2/\omega_{ce}^2 = 0.5$. Tsang [24] considered this effect, but only for large values of Δ_h where he did not see complete stabilization.

By comparison, the whistler waves can have growth rates that are larger by two orders of magnitude if the anisotropy exceeds a critical value, which is about three for parameters characteristic of hot-electron plasmas formed by ECH. Indeed, whistler growth rates can be reduced to low values mainly by increasing the average energy of the hot electrons and decreasing the temperature anisotropy. These two effects are illustrated in Figs 9a and 9b, in a single-species hot-electron plasma with $\ell = 0$, $\eta = 3$ and $\beta = 30\%$. The average perpendicular energy is expressed as $\epsilon_\perp = T_h/mc^2$; in Fig. 9b, $\epsilon_\perp = 1$. Finally, we evaluate the whistler growth rates in a two-component equilibrium obtained from the Fokker-Planck ECH model: $T_h = 527$ keV, $\Delta_h = 30\%$, $T_c = 800$ eV, $\omega_{pe}^2/\omega_{ce}^2 = 0.5$ and $\beta = 31\%$. The temperature anisotropy has been varied ($\eta = 3, 6, 10, 20$) to show the rapid decrease in growth rate for decreasing anisotropy, as displayed in Fig. 10a. For the weakly unstable whistler waves the growth is convective. It is thus of interest to evaluate the spatial amplification rates k_i, as illustrated in Fig. 10b.

4. DISCUSSION AND CONCLUSIONS

We have demonstrated several points in this paper. First of all, using the classical Fokker-Planck model of ECH, it is possible to reproduce all of the features of the SM-1 experimental results that can be compared with the reduced one-dimensional model. In particular, there is no need to invoke collective processes, such as

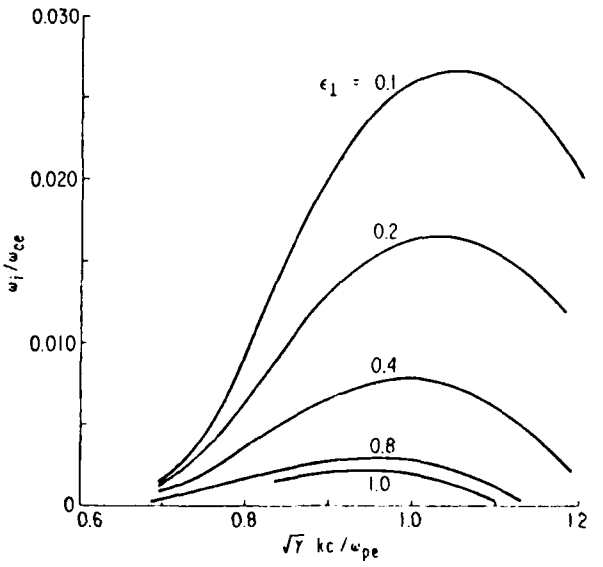

FIG. 9a. Whistler mode growth rates for fixed anisotropy, $\eta = 3$, and different values of the average hot-electron energy. The plasma parameters are specified in the text.

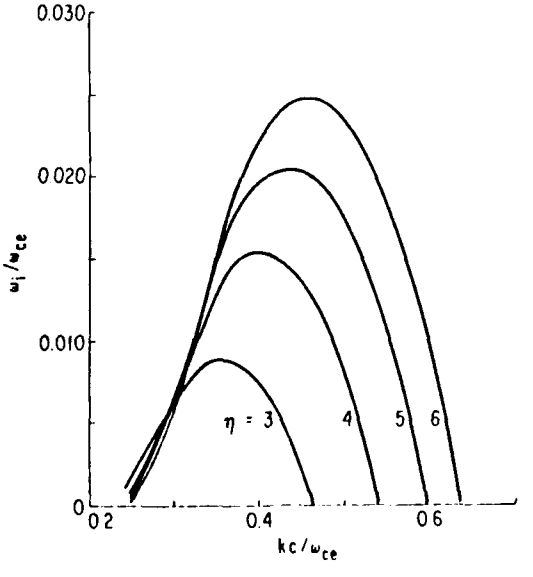

FIG. 9b. Whistler mode growth rates for fixed average hot-electron energy, $\epsilon_\perp = 1$, and different values of the temperature anisotropy

unstable whistler waves, to provide a self-consistent picture of the hot-electron distribution in energy and the RF power density required to sustain it. This property of the present Fokker–Planck model is in contrast to the moment approach of Hamasaki et al. [11], as one might expect from the non-Maxwellian character of the hot-electron equilibrium distribution. An interesting possibility is suggested by these results, namely that a different class of test distribution functions, similar to those obtained here, could be used in the moment approach to obtain useful analytic descriptions of ECH equilibria.

The numerical description obtained in the present work also contributes to clarifying the role of non-adiabatic scattering in limiting the hot-electron energy and it reveals in quantitative terms the importance of the microwave integrity of the cavity in which the ECH is carried out. For single-frequency heating it is apparently necessary to have a high enough cavity quality factor to permit the ordinary mode field strength to exceed by a large factor the extraordinary mode electric field strength. Similarly, UORH can only be expected to yield the high energy densities observed in ELMO if the UORH field strengths can approach values of the order of 10^2 V·cm^{-1}, while the corresponding absorbed power densities remain around 1 W·cm^{-3} or less.

These results are of practical importance in designing experimental ECH approaches to achieving relativistic-electron plasmas; but they also suggest that the reduced Fokker–Planck model can provide a useful simplified description of other plasmas in which ECH may occur, such as magnetospheric plasmas.

For our immediate purposes, the reduced Fokker–Planck model provides a detailed, self-consistent description of hot-electron plasmas that can be analysed for stability. In keeping with a large body of empirical observations, we find that whistler waves are likely to be unstable unless the temperature anisotropy is reduced and the hot-electron energy is increased. Cyclotron maser modes are shown to be suppressed by the cold background electrons that normally make up the majority species in an ECH plasma.

In a recent PhD thesis, Garner [29] has studied the characteristics of microinstabilities in an ECH plasma produced in a magnetic well configuration by single-frequency heating. Garner finds that the hot-electron component, whose temperature is 400 keV, is remarkably stable; the observed unstable whistler waves are apparently driven by a distinct group of warm electrons at a temperature around 2 keV. The third electron component is a cold population at a temperature

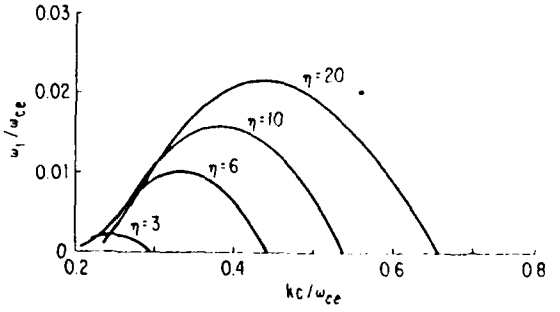

FIG. 10a. Whistler mode temporal growth rates for a Fokker–Planck ECH equilibrium with ad hoc values of the temperature anisotropy.

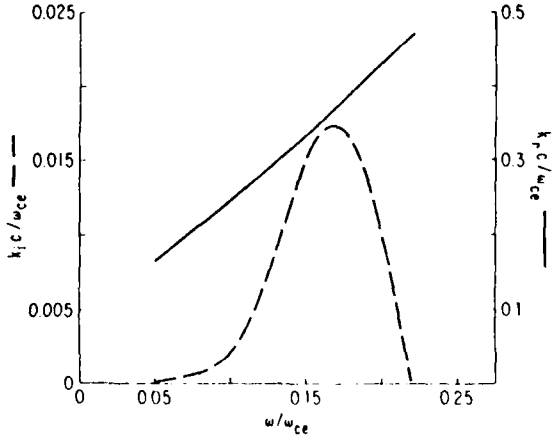

FIG. 10b. Whistler mode spatial growth rates and propagation vector for the Fokker–Planck ECH equilibrium with $\eta = 3$.

around 100 eV. The cold-, warm- and hot-electron densities are roughly equal and are in the range of $(1\text{–}2) \times 10^{11}$ cm^{-3}. Garner's thesis contains an interesting speculation regarding the observed stability of the hot-electron group that is not predicted by his analyses, namely that, if stochastic heating can occur at energies above the predicted threshold for super-adiabatic electron behaviour, the resulting distribution of hot electrons might indeed be stable at high temperatures. Our kinetic model of the relativistic heating process assumes that stochastic heating is maintained by the overlap of relativistic, Doppler-shifted resonances, and our analysis of the resulting equilibria demonstrates the relativistic stabilization of whistler waves as well as the cold-electron stabilization of the fast-wave branch of the electromagnetic mode. The distinct warm-electron component can be minimized or even eliminated by the use of O-mode heating or UORH, as shown by the present Fokker–Planck results.

APPENDIX

In brief, our picture of particle balance in mirror-confined ECH plasmas is as follows:

A-1. Low-energy processes

At energies $\epsilon \lesssim 100$ eV, particle balance is maintained by three dominant processes, namely (i) ionization of ambient neutral gas, (ii) free flow of cold ions along the magnetic lines of force and out the ends of the magnetic mirror, and (iii) electrostatic confinement of electrons in an ambipolar potential well whose depth Φ is governed by the electron heating rate $\dot{\epsilon}$ and the cold-ion escape rate.

Equating the ion and electron confinement times yields

$$e\Phi \simeq L\dot{\epsilon}/v_i$$

where v_i is the cold-ion flow velocity and L is the length of the plasma column. Furthermore, the escape of these electrons and cold ions is balanced by ionization, so that

$$v_i/L \simeq n_0\langle\sigma_{ionization}v_e\rangle$$

where n_0 is the density of neutral gas in the plasma. Under typical conditions, the characteristic rates for these three processes are around $5 \times 10^4\ s^{-1}$.

A-2. Intermediate-energy processess

In the energy range 100 eV $\lesssim \epsilon \lesssim$ 10 keV, the dominant dynamical processes are Coulomb scattering and ECH. The Coulomb scattering causes both slowing-down and pitch-angle scattering of heated electrons. For energy balance, the slowing-down must be offset by ECH for energies above a relatively low critical energy $\epsilon \gtrsim \epsilon_1 \simeq 3e\Phi$:

$$|\dot{\epsilon}_{RF}(\epsilon_1)| = |\dot{\epsilon}_{Coul}(\epsilon_1)|$$

Using rudimentary formulas for each rate, we obtain

$$\frac{\pi eE_{RF}^2}{2B_0M_t}\left(\frac{M-1}{M_t-1}\right)^{1/2}K^{-1}\left(\frac{M_t-1}{M-1}\right)$$

$$= \frac{n_e \ln\Lambda}{1.3\times10^5\,\epsilon_1^{1/2}}\ \frac{eV^{3/2}\,cm^3}{s}$$

For typical values of the ECH electric field, $E_{RF} \simeq 10$–$20\ V\cdot cm^{-1}$, the central magnetic field, $B_0 \simeq 3$ kG, the electron density, $n_e \simeq 5\times10^{11}\ cm^{-3}$, the overall mirror ratio, $M \simeq 2$, and the mirror ratio at the test electron turning point, $M_t = 1.7$, the critical electron energy for runaway, ϵ_1, can be just above 100 eV. (Here, K is the elliptic integral associated with the electron bounce motion.)

Simultaneously, with ECH, small-angle Coulomb collisions scatter heated electrons into the loss cone at a rate given by

$$\left(\frac{d\theta^2}{dt}\right) \simeq 1.5\times10^{-6}\,\frac{n_e \ln\Lambda}{\epsilon^{3/2}}\ \frac{eV^{3/2}\,cm^3}{s}$$

The corresponding rate of pitch-angle diffusion associated with ECH is given by

$$\left(\frac{d\theta^2}{dt}\right)_{RF} \simeq \frac{\pi}{8}\frac{eE_{RF}^2}{B_0\epsilon}\left(\frac{M_t}{M_{res}}-1\right)^2$$

$$\times\left(\frac{M-1}{M_t-1}\right)^{1/2}\frac{K^{-1}\left(\frac{M_t-1}{M-1}\right)}{M_t(M_t-1)}$$

where M_{res} is the mirror ratio at the resonant surface. Since $\dot{\theta}_{RF} \simeq \epsilon^{-1}$, while $\dot{\theta}_{Coul} \simeq \epsilon^{-3/2}$, RF-driven pitch-angle diffusion may dominate at high energies, $\epsilon > \epsilon_2 \simeq 10$ keV, typically. In the intermediate energy range, $\epsilon_1 \lesssim \epsilon \lesssim \epsilon_2$, Coulomb scattering is typically the dominant loss process. The resulting pitch-angle displacement of an electron with initial pitch angle θ_i can be estimated from

$$\Delta\theta \simeq \int_{\epsilon_1}^{\epsilon_2}\frac{\dot{\theta}_{Coul}}{\dot{\epsilon}_{RF}}\,d\epsilon$$

Since $\dot{\epsilon}_{RF}$ is almost independent of energy in this range, we have

$$\frac{\Delta\theta}{\theta_i} \simeq \frac{1.5\times10^{-6}\,n_e \ln\Lambda}{\theta_i^2\,\dot{\epsilon}_{RF}}$$

$$\times\ \frac{eV^{3/2}\,cm^3}{s}\int_{\epsilon_1}^{\epsilon_2}d\epsilon\,\epsilon^{-3/2}$$

$$= \frac{3\times10^{-6}\,n_e \ln\Lambda}{\theta_i^2\,\dot{\epsilon}_{RF}}\left(\epsilon_1^{-1/2}-\epsilon_2^{-1/2}\right)\frac{eV^{3/2}\,cm^3}{s}$$

Typically, $(\Delta\theta/\theta_i) \ll 1$, provided the heating rate is sufficiently large, for example $\dot{\epsilon}_{RF} \leq 10^7$ eV·s^{-1}. Some of the runaway electrons will indeed be lost, especially for $\epsilon \gtrsim \epsilon_1$, but the fractional hot-electron density obtained from energy balance alone provides a useful estimate of an upper bound on this ratio. Note also that in the one-dimensional Fokker-Planck model we define the hot-electron density as consisting only of electrons with energies above a specified value, which is usually chosen as 20 keV. For $\epsilon > 20$ keV, the RF-driven pitch-angle diffusion typically exceeds pitch-angle scattering due to Coulomb collisions; the loss rate of heated electrons in this energy range is estimated to be very small. Since we specify the total electron density in the one-dimensional model and restrict the hot-electron component to those electrons for which Coulomb scattering is negligible, we expect the relative hot-electron density obtained from energy balance considerations to be a valid upper bound and a close estimate.

A-3. High-energy processes

In the energy range $\epsilon > 10$ keV, Coulomb scattering pitch-angle diffusion into the loss cone can typically be offset by RF-driven pitch-angle diffusion in which heated electrons diffuse *towards* the resonant surface (where $\omega_{RF} = NeB/\gamma m$, N = 1, 2, 3,...). Heating at the second and higher harmonics of the relativistic-electron gyrofrequency plays a major role in the maintenance of efficient stochastic heating and causes further pitch-angle diffusion towards the midplane of the magnetic mirror, $\theta = \pi/2$. Particle losses in this energy region are very small, and energy balance is dominated by relativistic ECH and synchrotron radiation up to the energy at which electrons cease to be adiabatic. The escape of a very small number of very high energy electrons has little effect on particle balance, but can completely offset continued heating to higher energies.

In summary, we suggest that the justification of separating energy balance and particle balance conditions rests on the smallness of $(\Delta\theta/\theta)$, as estimated above, as well as on the unusual nature of the RF-driven pitch-angle diffusion that tends to drive heated electrons back towards the resonant surface. We have attempted to minimize the impact of particle balance processes on our one-dimensional Fokker-Planck model by regarding only electrons with energies above 20 keV as 'hot electrons' and specifying the total density ab initio.

ACKNOWLEDGEMENT

This work was supported by the United States Air Force Office of Scientific Research, under Contract No. F49620-86-C-0055.

REFERENCES

[1] BECKER, M.C., DANDL, R.A., EASON, H.O., ENGLAND, A.C., KERR, R.J., ARD, W.B., Nucl. Fusion: 1962 Suppl., Part 1 (1962) 345.
ARD, W.B., DANDL, R.A., STETSON, R.F., Phys. Fluids **9** (1966) 1498.
[2] DANDL, R.A., EASON, H.O., EDMONDS, P.H., ENGLAND, A.C., Nucl. Fusion **11** (1971) 411.
[3] DANDL, R.A., GUEST, G.E., "The ELMO Bumpy Torus", Fusion, Vol. 1, Part B (TELLER, E., Ed.), Academic Press, New York (1981) 79.
[4] HOT-ELECTRON Ring Physics (Proc. 2nd Workshop San Diego, CA, 1981), Vols 1 and 2, CONF-811203, Oak Ridge National Laboratory (1982) (available from National Technical Information Service, United States Department of Commerce, Springfield, VA.)
[5] FURTH, H.P., BOOZER, A.H., The EST (ELMO Snaky Torus), personal communication (1982);
MILLER, R.L., Phys. Fluids **29** (1986) 1176.
[6] ROSENBLUTH, M.N., TSAI, G.T., VAN DAM, J.W., ENQUIST, M.G., Phys. Rev. Lett. **51** (1983) 1967.
[7] GRAWE, H., Plasma Phys. **11** (1969) 151.
[8] HOWARD, J.E., Plasma Phys. **23** (1981) 597.
[9] BATCHELOR, D.B., GOLDFINGER, R.C., Nucl. Fusion **20** (1980) 403, and references cited therein.
[10] BERNSTEIN, I.B., BAXTER, D.C., Phys. Fluids **24** (1981) 108.
[11] HAMASAKI, S., KRALL, N.A., SPERLING, J.L., Nucl. Fusion **23** (1983) 571.
[12] KILLEEN, J., KERBEL, G.D., McCOY, M.G., MIRIN, A.A., Computational Methods for Kinetic Models of Magnetically Confined Plasmas, Springer, New York (1986).
[13] KERBEL, G.D., McCOY, M.G., Phys. Fluids **28** (1985) 3629.
[14] GUEST, G.E., MILLER, R.L., CHANG, C.S., Nucl. Fusion **27** (1987) 1245.
[15] QUON, B.H., DANDL, R.A., DIVERGILIO, W., GUEST, G.E., LAO, L.L., LAZAR, N.H., SAMEC, T.K., WUERKER, R.F., Phys. Fluids **28** (1985) 1503.
[16] UCKAN, N.A., Phys. Fluids **25** (1982) 2381, and references cited therein.
[17] SUDAN, R.N., Phys. Fluids **6** (1963) 57.
[18a] CHU, K.R., HIRSHFIELD, J.L., Phys. Fluids **21** (1978) 461.
[18b] PRITCHETT, P.L., Phys. Fluids **29** (1986) 2919.
[19] GLADD, N.T., Phys. Fluids **26** (1983) 974;
HEDRICK, C.L., Convective-Absolute Boundary for Whistler Modes, Rep. ORNL-TM-3143, Oak Ridge National Laboratory (1970).
[20] GUEST, G.E., MILLER, R.L., CAPONI, M.Z., Phys. Fluids **29** (1986) 2556.

[21] STOTLER, D.P., BERK, H.L., ENGQUIST, M.G., Phys. Fluids **29** (1986) 1149, and references cited therein.
[22] GUEST, G.E., SIGMAR, D.J., Nucl. Fusion **11** (1971) 151.
[23] GUEST, G.E., DORY, R.A., Phys. Fluids **8** (1965) 1853; DORY, R.A., GUEST, G.E., HARRIS, E.G., Phys. Rev. Lett. **14** (1965) 131.
[24] TSANG, K., Phys. Fluids **27** (1984) 1659.
[25] HARRIS, E.G., J. Nucl. Energy, Part C, Plasma Phys. **2** (1961) 138;
KRALL, N.A., TRIVELPIECE, A.W., Principles of Plasma Physics, McGraw-Hill, New York (1973) 414 ff.
[26] FRIED, B.D., CONTE, S.D., The Plasma Dispersion Function, Academic Press, New York (1961).
[27] ABRAMOWITZ, M., STEGUN, I.A. (Eds), Handbook of Mathematical Functions, 10th edn, United States Government Printing Office, Washington, DC (1972) 889.
[28] LAU, Y.Y., CHU, K.R., Phys. Rev. Lett. **50** (1983) 243.
[29] GARNER, R.C., Electron Microinstabilities in an ECRH, Mirror-Confined Plasma, PhD Thesis; Rep. PFC/RR-86-23, Massachusetts Institute of Technology, Cambridge (1986).

(Manuscript received 2 March 1987
Final manuscript received 12 October 1987)

Amplification of whistler waves propagating through inhomogeneous, anisotropic, mirror-confined hot-electron plasmas

G. E. Guest and R. L. Miller
Applied Microwave Plasma Concepts, Inc., Carlsbad, California 92009

(Received 15 April 1988; accepted 18 August 1988)

A fully relativistic local dispersion relation for whistler waves has been solved at closely spaced points along the magnetic field lines of a 2:1 magnetic mirror in which a highly anisotropic, spatially inhomogeneous, hot-electron plasma is confined. The limiting plasma parameters for convective (spatial) growth have been determined numerically and used to identify plasma conditions leading to maximum amplification of input microwave signals introduced in the form of whistler waves. The maximum gain has been evaluated numerically for a range of values of the hot-electron plasma within which all major stability criteria are satisfied. Very high gains (~ 40 dB) are indicated over the entire range of beta investigated.

I. INTRODUCTION

It is well known that whistler waves can be unstable in mirror-confined hot-electron plasmas because of the pressure anisotropy inherent in magnetic-mirror confinement.[1] Indeed, the phenomenon of unstable whistler waves has often been invoked to interpret spontaneous rf emissions from laboratory[2] and space plasmas,[3] and has recently been proposed as a way of transforming the energy stored in mirror-confined hot-electron plasmas into giant pulses of high-powered microwave radiation.[4,5] The proposed transformation results from the amplification of whistler waves propagating along magnetic lines of force and passing through the anisotropic, hot-electron plasma. Here we investigate the maximum gain that a whistler can undergo in a spatially inhomogeneous plasma, confined in a magnetic-mirror field of finite spatial extent.

Because the whistler instability mechanism depends on the kinetic properties of the hot-electron equilibrium, particularly the distribution of electrons in velocity space, theoretical analyses of the growth typically use idealized, spatially uniform models of the plasma in order to treat the velocity-space issues realistically.[1] Under these idealized conditions, growth of the whistler wave can be either convective or absolute, depending on the plasma parameters.[6] Absolutely unstable or temporally growing waves are expected to spread throughout the unstable plasma and grow in amplitude until quasilinear or nonlinear processes balance the destabilizing conditions. By contrast, the growth of convectively unstable or spatially amplifying waves may be limited by the finite transit time of a wave packet across the finite spatial extent of the unstable plasma as well as by the spatial nonuniformity of the confining magnetic field, rather than quasilinear or nonlinear mechanisms.

In the present study we use linearized theories to determine the overall gain, $G(\omega)$, experienced by a pulse of microwave power launched at one end of a mirror-confined, hot-electron plasma and propagating along the magnetic lines of force in the form of whistler waves:

$$G(\omega) \equiv |E^2_{\text{out}}(\omega, z = +L)|/|E^2_{\text{in}}(\omega, z = -L)|.$$

Here ω is the (radian) frequency of the wave launched at the axial position $z = -L$ with rf electric field strength E_{in}. After a single transit through the plasma, the wave arrives at the axial position $z = L$ with amplitude E_{out}. Since this procedure will yield the desired gain only if the unstable growth is convective, we have carried out a detailed numerical evaluation of the threshold conditions for absolute growth and restricted the range of plasma parameters to lie entirely within the convectively unstable range.

Apart from transients at the beginning and end of each pulse, the input wave amplitude is assumed to be constant in time throughout the pulse; and the spatial and temporal behavior of the wave can be determined using Fourier and Laplace transformed equations in the conventional way.[6] When inverting the transformed variables it is necessary to displace the Laplace integral path to the real-ω axis while deforming the Fourier inversion path to prevent any zeros of the dispersion relation from crossing the deformed path of integration in the complex k plane, where k is the (parallel) wavenumber. As is well known, this procedure is only possible if the whistler wave growth is convective; in the case of absolute growth, two poles from opposite halves of the complex k plane merge.

To ensure that we consider only convectively unstable cases, we have evaluated the threshold conditions for absolute (temporal) growth for the hot-electron equilibria under investigation. For hot-electron plasmas created by electron cyclotron heating (ECH), the convective/absolute boundary can be conveniently represented in two dimensions by fixing some of the plasma parameters in ways that reflect fundamental properties of the ECH process. Thus, for example, the total plasma density is usually limited by microwave cutoff so that $\omega^2_{pe}/\omega^2_{\mu} \leq 1$. Here ω_{pe} and ω_{μ} are the electron plasma and microwave frequencies, respectively. Moreover, the relative density of hot electrons $n_h/n \equiv \Delta$ may be limited by the onset of flutelike instabilities in simple magnetic-mirror configurations; although no such limitation occurs in magnetic "well" configurations with favorable curvature of the magnetic lines of force. Even in such a flute-stable configuration, however, the plasma pressure may be limited by equilibrium conditions such as the so-called "mirror mode," and the value of hot-electron beta, $\beta = 2\mu_0 P_h/B^2$, may be limited in inverse proportion to the anisotropy.[7] Here B is the magnetic intensity and μ_0 is the permeability of free space.

 0031-9171/88/123690-07$01.90

If no other stability criteria are violated, the gain $G(\omega)$ can be evaluated up to the threshold conditions defined by the C/A boundary in a straightforward way; this is the main objective of the work described here. The gain is then given directly by

$$G(\omega) = \exp\left(-2 \int_{L_-}^{L_+} k_i(\omega,z)dz \right),$$

where k_i is the imaginary part of the wave vector corresponding to solutions of the local dispersion relation with real frequency ω.

In order to account for the z-dependent equilibria confined in finite sized magnetic-mirror configurations we adopt simple model equilibria with hot-electron distribution functions mapped along magnetic field lines through adiabatic invariants. The properties of these equilibria are summarized briefly in Sec. II. A fully relativistic dispersion relation is then used to evaluate the C/A boundary for whistler waves. The dispersion relation, while fully relativistic, can give only a local evaluation of the wave properties, since it is derived under the assumptions of spatial uniformity. This procedure is expected to yield a valid description provided the scale length for variation of the plasma equilibrium is much greater than the wavelength of the whistler waves. Since we are primarily interested in quasioptical systems with scale lengths much larger than wavelengths, this condition is not particularly restrictive. In effect, we are constructing a WKB solution from numerical solutions of the local dispersion relation within plasma parameter ranges for which the unstable growth is guaranteed to be convective. The numerical analysis of the dispersion relation and typical results are recapitulated in Sec. III. The gain is then evaluated from real-ω solutions of the dispersion relation in a way that is discussed at some length in Sec. IV. Several cases are presented there in which the temperature anisotropy and hot-electron beta are varied so as to move along a particular C/A boundary (corresponding to a fixed relative hot-electron concentration, $\Delta = 30\%$). Substantial values of the gain are indicated for hot-electron plasmas of typical laboratory dimensions.

The major findings are summarized in Sec. V, and the nature of these findings is discussed. In particular, the unresolved issue of the role of quasilinear or nonlinear processes is given some emphasis because of the indications that the maximum gain predicted in the linear theory varies only weakly with beta and remains large in plasmas with high energy densities, where saturation levels of output power might be expected to be very high.

II. THE MODEL EQUILIBRIA

In this section we summarize the way in which the equilibrium properties of the plasma depend on distance along the magnetic lines of force. Local properties of electron cyclotron heated hot-electron plasmas have been discussed extensively,[7] and a few studies have attempted to model the axial dependence in nonrelativistic formulations of the hot-electron dynamics. Here we follow the conventional approach to mapping relativistic-electron equilibria along magnetic lines of force assuming the invariance of the total energy ϵ, and the magnetic moment μ:

$$\epsilon = mc^2(\gamma - 1) = mc^2\left[\sqrt{1 + (u^2/c^2)} - 1\right]$$

and

$$\mu = (m\mu_i^2)/(2B).$$

In these expression, γ is the relativistic Lorentz factor and $\mathbf{u}$ is the momentum per unit rest mass with components $u_\perp$ and $u_\parallel$ perpendicular and parallel, respectively, to the magnetic field $\mathbf{B}$. Here m is the electron rest mass and c is the speed of light in vacuum.

The relative intensity of the steady magnetic field is assumed to vary along the line of force of interest as follows:

$$b = \frac{B(z)}{B(0)} = \left(\frac{M+1}{2}\right) - \left(\frac{M-1}{2}\right)\cos\left(\frac{\pi z}{L}\right).$$

Here $z = 0$ defines the so-called "midplane" on which the magnetic intensity reaches its minimum value $b = 1$, while $z = L$ defines the so-called "mirror throat," where B reaches its maximum value $b = M$, the mirror ratio.

The cold-electron component, which typically contains the majority of electrons, will be modeled as an isotropic, pressureless fluid whose density is independent of z. By contrast, the hot-electron component is assumed to be anisotropic and relativistic and described by a distribution function of the form[8]

$$f_h(u_\perp^2,u_\parallel^2,z) = \begin{cases} \sum_{l=0}^{\infty} C_h^{(l)}\left(\frac{u_\perp^2}{b\alpha_\perp^2}\right)^l \exp\left\{ -\left(\frac{u_\parallel^2}{\alpha_\parallel^2} + (b-1)\frac{u_\perp^2}{b\alpha_\parallel^2} + \frac{u_\perp^2}{b\alpha_\perp^2}\right)\right\}, & \text{outside of the loss cone,} \\ 0, & \text{inside the loss cone.} \end{cases} \quad (1)$$

If $\mathbf{u}_0$ is the momentum per unit rest mass evaluated at the midplane $z = 0$, then in terms of the constants of motion,

$$u_{0\parallel}^2 = u^2 - 2\mu B_0/m = u_\parallel^2(z) + (b-1)\left[u_\perp^2(z)\right]/b \quad (2)$$

and

$$u_{0\perp}^2 = 2\mu B_0/m = u_\perp^2/b. \quad (3)$$

Here $u_{0\parallel}$ and $u_{0\perp}$ are the components of $\mathbf{u}_0$ parallel and perpendicular, respectively, to the static magnetic field.

A z-dependent loss cone in $\mathbf{u}$ space is defined by setting

$u_\parallel^2(L) = 0$:

$$u_\parallel^2(L) = u^2 - 2\mu B_{\max}/m = 0$$
$$= u_\parallel^2(z) + u_\perp^2(z) - u_\perp^2(z)B_{\max}/B(z),$$

or

$$\left(\frac{u_\parallel^2(z)}{u_\perp^2(z)}\right)_{\text{loss cone}} = \frac{B_{\max}}{B(z)} - 1 = \frac{M}{b} - 1. \tag{4}$$

If we now collect terms in $u_\perp^2(z)$ in the exponential factor we have

$$f_h(u_\perp^2, u_\parallel^2, z) = \sum_{l=0}^{\infty} C_h^{(l)} \left(\frac{u_\perp^2}{b\alpha_\perp^2}\right)^l \exp\left(-\frac{u_\parallel^2}{\alpha_\parallel^2} - \frac{u_\perp^2}{\alpha_\perp^2(z)}\right),$$
$$\text{if } \frac{u_\parallel^2}{u_\perp^2} \leq \frac{M}{b-1}, \tag{5}$$
$$= 0, \quad \text{if } \frac{u_\parallel^2}{u_\perp^2} > \frac{M}{b-1},$$

where

$$\alpha_\perp^2(z) = (\alpha_{\perp 0}^2 \alpha_\parallel^2 b)/[\alpha_{\perp 0}^2(b-1) + \alpha_\parallel^2],$$

or, if $\eta \equiv \alpha_{\perp 0}^2/\alpha_\parallel^2$,

$$\alpha_\perp^2(z) = \eta b \alpha_\parallel^2/[\eta(b-1) + 1]. \tag{6}$$

The z-dependent hot-electron density is now given by

$$n_h(z) = \sum_{l=0}^{\infty} C_h^{(l)} \pi \int_{-\infty}^{\infty} du_\parallel \exp\left(-\frac{u_\parallel^2}{\alpha_\parallel^2}\right)$$
$$\times \int_{bu_\parallel^2/(M-b)}^{\infty} du_\perp^2 \left(\frac{u_\perp^2}{b\alpha_\perp^2}\right)^l \exp\left(-\frac{u_\perp^2}{\alpha_\perp^2(z)}\right), \tag{7}$$

and for the simple bi-Gaussian distribution, $l = 0$, we have

$$n_h(z) = \pi^{3/2} \alpha_\perp^2(z) \alpha_\parallel C_h^{(0)} \{1 + [\alpha_\parallel^2/\alpha_\perp^2(z)]$$
$$\times [b/(M-b)]\}^{-1/2} \tag{8}$$

or

$$\frac{n_h(z)}{n_h(0)} = \frac{\alpha_\perp^2(z)}{\alpha_{\perp 0}^2}\left(1 + \frac{(\alpha_{\perp 0}^2/\alpha_{\parallel 0}^2)[1/(M-1)]}{1 + [\alpha_\parallel^2/\alpha_\perp^2(z)][b/(M-b)]}\right)^{-1/2}$$
$$= \frac{b}{\eta(b-1)+1}\sqrt{\frac{(M-b)}{(M-1)}}. \tag{9}$$

An illustrative case is shown in Fig. 1 for a mirror ratio $M = 2$ and two different temperature anisotropies, $\eta = 5$ and 20. The z-dependent relative magnetic intensity b is shown, together with the z-dependent relative hot-electron densities for the two different temperature anisotropies. The figure indicates the degree to which higher temperature anisotropy is associated with increased peaking of the hot-electron density at the midplane. This property of the equilibria will be shown to have a major impact on the overall gain of a whistler wave propagating along the magnetic line of force. In quantitative terms, the z dependence of hot-electron density is given by

$$\frac{d}{dz}\frac{n_h(z)}{n_h(0)} = \frac{db}{dz}\left(\frac{(1-\eta)}{[1+\eta(b-1)]^2}\sqrt{\frac{(M-b)}{(M-1)}}\right.$$
$$\left. - \frac{b}{2\sqrt{(M-1)(M-b)}}\frac{1}{1+\eta(b-1)}\right)$$
$$\to \frac{db}{dz}\left(1 - \eta - \frac{1}{2(M-1)}\right), \quad \text{as } b \to 1. \tag{10}$$

Although it is not included in Fig. 1, the temperature anisotropy also decreases with distance from the midplane as

$$\frac{\alpha_\perp^2(z)}{\alpha_\parallel^2} = \frac{\eta b}{1+\eta(b-1)},$$

so that

$$\frac{d\alpha_\perp^2}{dz} = \frac{\alpha_\parallel^2 \eta b'(1-\eta)}{[1+\eta(b-1)]^2}. \tag{11}$$

Thus both temperature anisotropy and the relative hot-electron density decrease with distance away from the midplane, so that maximum amplification will occur at the midplane.

In contrast to this strong z dependence of the hot-electron density, the cold-electron density is expected to remain nearly constant in z, except for the spatial compression associated with the increasing magnetic intensity. The real value of $k(\omega)$ is determined mainly by the cold-plasma density and the magnetic intensity, and is slowly varying along the magnetic field lines.

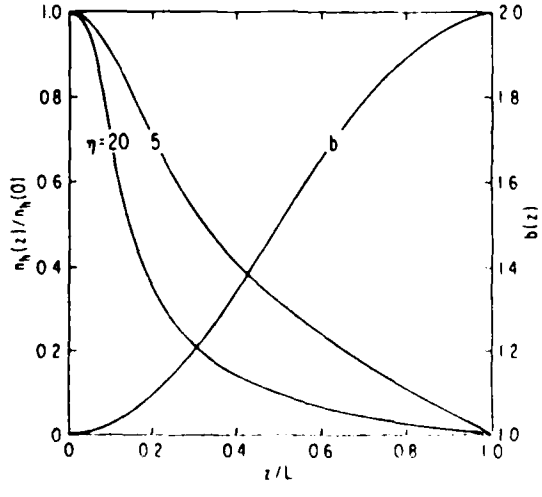

FIG. 1. Variation of relative hot-electron density and magnetic intensity, b, with distance along a magnetic field line.

III. CONDITIONS FOR MAXIMUM GAIN

The maximum amplification of an externally launched whistler wave is likely to be achieved in hot-electron plasmas that are just below the threshold for absolute or temporal growth. This threshold is frequently referred to as the C/A boundary, which is a hypersurface in a space spanned by the plasma parameters. On one side of this boundary only convective or spatial growth is possible, while on the opposite side of the boundary, absolute or temporal growth occurs. Thus, in order to explore the maximum gain that can be achieved, it is first necessary to define the C/A boundary in

terms of equilibrium parameters representative of physically realizable plasmas. This section summarizes the results of a numerical determination of the C/A boundary for unstable whistler waves in hot-electron plasmas whose local properties are modeled by the class of infinite, homogeneous, relativistic-electron distribution functions cited earlier, namely,

$$f_s = \sum_{l=0}^{\infty} C_l \left(\frac{u_\perp}{\alpha_\perp}\right)^{2l} e^{-u_\parallel^2/\alpha_\parallel^2} e^{-u_\perp^2/\alpha_\perp^2}.$$

The general methodology adopted here for determining the C/A boundary has been discussed at length by Briggs[6] and consists ultimately in locating simultaneous solutions of the dispersion relation and its derivative with respect to k, the (complex) wavenumber, for real values of the frequency ω. This general methodology is implemented in our case through novel numerical techniques appropriate to the class of distribution functions used here. These techniques have been fully described by Guest and Miller.[9]

It has been well established by many investigators[1] that the growth rate of unstable whistler waves increases with increasing values of the temperature anisotropy and the hot-electron beta, where beta is the ratio of the kinetic pressure nT to the magnetostatic pressure $B^2/2\mu_0$. For hot-electron plasmas created by electron cyclotron heating (ECH), several fundamental aspects of the heating and confinement processes limit the physically accessible values of beta and anisotropy in ways that can usefully restrict the range of plasma parameters to be considered here.[7,9] For example, effective penetration of the ECH power typically limits the maximum (total) electron density to values such that $\omega_{pe}^2 \lesssim \omega_\mu^2$, where ω_μ is the angular frequency of the ECH power. Typically, the relative fraction of electrons heated to high energies, $\Delta = n_h/n$, is much less than unity. Idealized theories of flutelike instabilities have been used to estimate critical values of Δ set by thresholds for occurrence of flutelike or ballooning modes: $\Delta_{crit} \sim 0.3$. Relativistic effects appear to increase this substantially, but we will usually assume $\Delta \lesssim 0.5$. In small magnetic mirrors, nonadiabatic effects can limit the maximum hot-electron energy to values such that $\rho \lesssim 0.05L$. Here ρ is the (relativistic) electron gyroradius and L is a characteristic scale length of the magnetic geometry. The condition for equilibrium, sometimes referred to as the mirror instability criterion, limits the product of anisotropy and beta, roughly as $\beta(\eta - 1) \lesssim 1$. For the anisotropic, hot-electron distribution functions used in the present work, a more accurate estimate of the beta limit corresponding to the mirror criterion can be obtained from the more general condition for existence of equilibria[10]:

$$\tau \equiv \frac{1}{\mu_0} + \frac{1}{B}\frac{dp_\perp}{dB} > 0. \tag{12}$$

In the nonrelativistic approximation, $p_\perp$, the component of plasma pressure perpendicular to the static magnetic field, is given by

$$p_\perp = mn\langle v_x^2 \rangle = mn\langle v_y^2 \rangle = mn\langle v_\perp^2/2 \rangle$$
$$= \pi \int_{-\infty}^{\infty} dv_\parallel \int_{v_{\perp m}}^{\infty} v_\perp \, dv_\perp \, f(v_\perp, v_\parallel) m v_\perp^2. \tag{13}$$

Here $v_{\perp 0}^2 = v_\parallel^2 b/(M-b)$ defines the loss cone at the point z where the local magnetic intensity is $B = bB_0$. Note that $v_{\perp 0}^2 \to 0$ as $M \to \infty$. If we use the bi-Maxwellian distribution function corresponding to $l = 0$[8] and evaluate the derivative of $p_\perp$ at the midplane, we obtain from the mirror criterion

$$\beta_{\perp 0} < \frac{\sqrt{M-1}(\eta^{-1} + M - 1)^{3/2}}{(M-1)(\eta - 1)(1.5\eta^{-1} + M - 1) - 3\eta^{-1}/8}, \tag{14}$$

where $\eta \equiv \alpha_\perp^2/\alpha_\parallel^2$. We have evaluated the limiting value of $\beta_\perp(\eta)$ for $M = 2$ and displayed this boundary in Fig. 2. Note that as $M \to \infty$ this criterion approaches

$$\beta_\perp(\eta - 1) \lesssim 1.$$

In Fig. 2 we show the value of anisotropy on the convective/absolute boundary $\eta_{c/a}$ as a function of $\beta_\perp$ for conditions that are appropriate to an ECH-generated hot-electron plasma. We have set $\omega_{pe}^2/\omega_{ce}^2 = 1$ and $\Delta = 0.3$, and varied $\bar{\gamma}$ to cover the indicated range of values of $\beta_\perp$. The associated values of $\bar{\gamma}$ are shown by the curve labeled $\bar{\gamma} - 1$. Here $\bar{\gamma}$ is the average of γ over the equilibrium distribution function, Eq. (5), in which only the $l = 0$ component is retained. The approximate mirror instability criteria $\beta(\eta - 1) = 1$ and $\tau = 0$ are also shown here; note that the C/A boundary lies slightly above the equilibrium limit for $\beta_\perp > 10\%$–20%. The nonrelativistic C/A boundary given by Iiyoshi *et al.*[11] is also shown for comparison with the fully relativistic numerical results. For a given value of $\beta_\perp$ the relativistic expressions indicate that slightly higher values of anisotropy are required for absolute growth.

The C/A boundary shown in Fig. 2 satisfies the conditions for physical accessibility identified here for $\beta_\perp \sim 10\%$–20% and thus will be used to estimate the maximum gain that can be achieved at lower values of beta. The results of

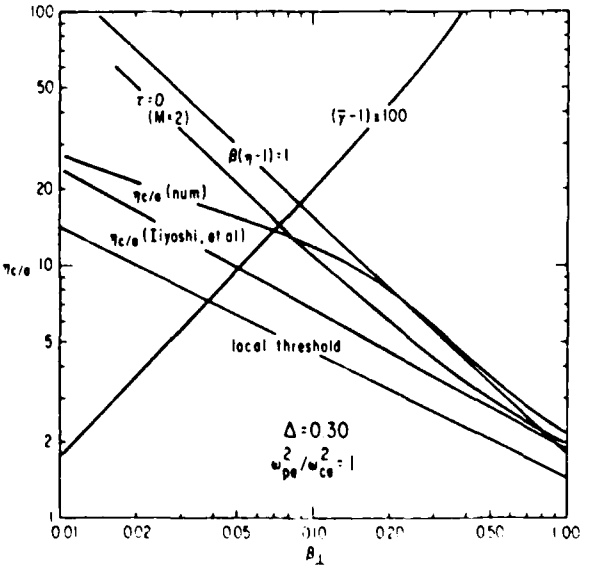

FIG. 2. Variation of anisotropy of the C/A boundary, $\eta_{c/a}$, and average hot-electron energy, $\bar{\gamma}$, with $\beta_\perp$, the perpendicular hot-electron beta. Here $\omega_{pe}^2/\omega_{ce}^2 = 1$ and $\Delta = 0.3$. Also shown is the mirror instability threshold

this evaluation of gain are described in Sec. IV.

We conclude the present section with one further set of results on the local wave properties of unstable whistlers at the C/A boundary shown in Fig. 2. These are displayed as functions of $\beta_\perp$ in Fig. 3, where we see that both the real and imaginary components of the propagation vector, together with the wave frequency, are decreasing functions of beta. This decrease reflects two underlying facets of the C/A boundary along which the parameters are evaluated, namely, that the maximum anisotropy for convective growth is decreasing with increasing values of beta, and that, in the present case, beta is being increased by increasing the average electron energy and hence the relativistic mass shift. The relativistic effects can be removed by holding the hot-electron energy fixed and varying beta by varying Δ. This procedure has been followed in generating the results shown in Figs. 4 and 5.

Figure 4 again shows the anisotropy at the C/A boundary as a function of beta, together with the corresponding values of Δ and the mirror instability criterion for $\bar{\gamma} = 1.4$. This value of $\bar{\gamma}$ corresponds to an average hot-electron energy just above 100 keV ($T = 111$ keV). Note that absolute growth is only possible for $\beta_\perp \geq 0.10$ corresponding to $\Delta = 0.155$, and that the C/A boundary drops below the mirror stability limit for $\beta_\perp > 0.17$ or $\Delta > 0.27$. The wave parameters along the C/A boundary are shown in Fig. 5, and here reflect only the decreasing value of anisotropy, as well as the increasing value of Δ. In the range that satisfies the mirror stability criterion, the wave parameters decrease only slightly, suggesting that relativistic effects are mainly responsible for the large decrease in wave parameters shown in Fig. 3.

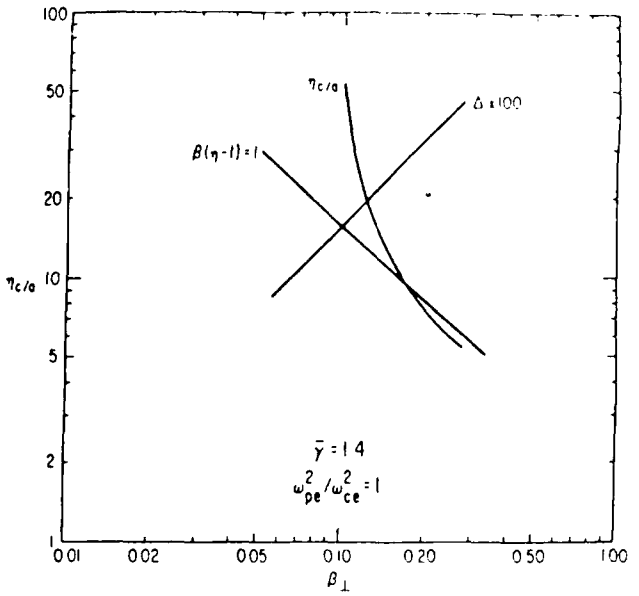

FIG. 4. The C/A boundary for fixed $\bar{\gamma} = 1.4$ and the relative hot-electron density, Δ, together with the mirror instability criterion

IV. EVALUATION OF MAXIMUM GAIN

We now estimate the maximum achievable gain for various plasma parameters by numerically evaluating the integral along magnetic field lines of the imaginary part of the propagation vector:

$$\ln G(\omega) = -2\int_{-l}^{l} k_i(\omega,z)\,dz. \tag{15}$$

This procedure is valid provided the growth is convective. We will examine a sequence of cases in which the plasma beta is increasing, and for each value of beta we will assume the maximum anisotropy for which the whistler growth is convective. Since the plasma density and anisotropy are greatest on the midplane, it is the midplane values of plasma

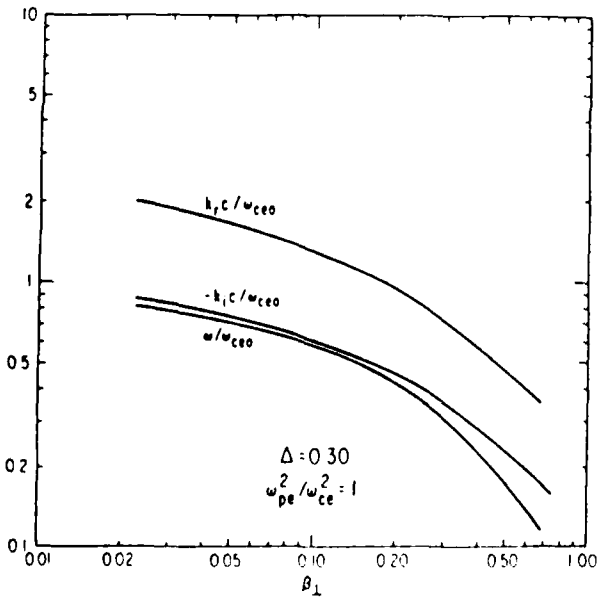

FIG. 3. Wave parameters versus $\beta_\perp$ for $\eta_{c/a}$ on the C/A boundary shown in Fig. 2

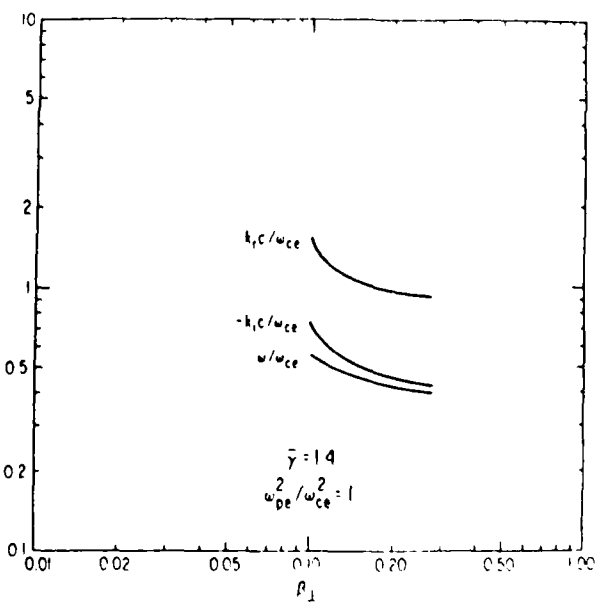

FIG. 5. Wave parameters along the C/A boundary for the cases shown in Fig. 4

and wave parameters on the C/A boundary that determine the maximum anisotropy and the corresponding wave frequency for each value of beta. The anisotropy and density are readily determined at each point along the magnetic field line; and the dispersion relation is then solved locally to obtain the complex propagation vector at that point for the frequency specified at the midplane. The gain integral is then evaluated numerically.

We have carried out this evaluation of the gain for $\beta_\perp \doteq 5\%$, 10%, 15%, 20%, and 25% in the case shown in Fig. 2: $\omega_{pe}^2/\omega_{ce}^2 = 1$, $\Delta = 0.30$, and $l = 0$. The magnetic geometry assumed was a fixed $M = 2$ magnetic mirror; and thus no attempt was made to relate the equilibrium value of the anisotropy to the shape of the magnetic field. We return to this point in Sec. V. The midplane parameters for the cases examined are tabulated in Table I. The series was terminated at $\beta_\perp = 25\%$ since the mirror instability criterion was not satisfied at the C/A boundary for greater values of $\beta_\perp$.

The last column of Table I gives the value of

$$I \equiv -\int_0^1 \left(\frac{k_i c}{\omega_{ce0}}\right)\left(\frac{dz}{L}\right).$$

The gain is then given by

$$G(\omega) = \exp[4(L\omega_{ce0}/C)I].$$

For typical conditions, the applied microwave power resonates with the second harmonic of the local electron gyrofrequency at the midplane. Thus

$$\omega_{ce0} = \pi f_\mu,$$

and we can estimate the scale factor as follows:

$$\frac{4L\omega_{ce0}}{c} \simeq \frac{4\pi L f_\mu}{c} = \frac{4\pi L}{\lambda_\mu},$$

where λ_μ is the free-space wavelength of the microwave heating power. In order of magnitude, $L/\lambda_\mu \geqslant O(10)$ for typical existing experimental devices. The indicated values of gain are then, again, in order of magnitude,

$$G(\omega) \sim O(10^4) \sim 40 \text{ dB}.$$

In addition to the peak growth rates shown in Table I we can readily estimate the effective bandwidth by calculating the total gain for whistler waves of varying frequencies propagating through a particular anisotropic, mirror-confined, hot-electron equilibrium. For definitiveness, we again choose the plasma parameters to be near the convective/absolute boundary for the center frequency of the unstable frequency band. Illustrative cases of $\beta_\perp = 5\%$, 10%, and 20% are shown in Fig. 6, where the dimensionless gain factor,

$$-\int_0^1 \left(\frac{k_i c}{\omega_{ce0}}\right)\frac{dz}{L},$$

is plotted against the frequency normalized to the center frequency. Note that the bandwidth increases as $\beta_\perp$ increases, i.e., as the average hot-electron energy increases. The full-width at half-maximum varies from roughly 0.15 at $\beta_\perp = 5\%$ to more than 0.25 at $\beta_\perp = 20\%$.

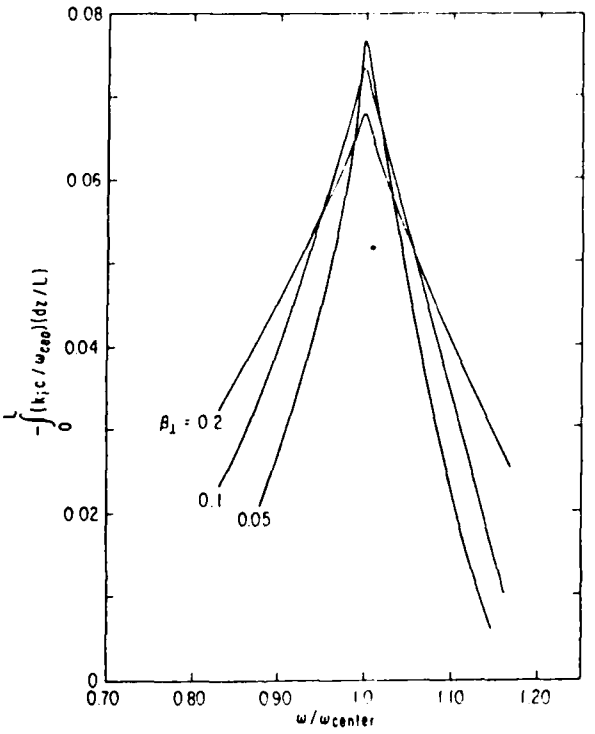

FIG. 6. The frequency-dependent gain factor, $-\int_0^1 (k_i c/\omega_{ce0})dz/L$, for whistler waves of varying frequency in hot-electron equilibria with temperature anisotropies near the convective/absolute boundary and $\beta_\perp = 5\%$, 10%, and 20%. Plasma and wave parameters for these three cases are listed in Table I.

Thus the linear theory suggests that very high gain is possible. It should be emphasized that the linear theory can-

TABLE I. Summary of the wave and plasma parameters at the C/A boundary for varying values of $\beta_\perp$. For all these cases, $\omega_{pe}^2/\omega_{ce}^2 = 1$ and $\Delta = 0.30$.

$\beta_\perp$ (%)	$\eta_{C/A}$	ω/ω_{ce0}	$k_r c/\omega_{ce0}$	$k_i c/\omega_{ce0}$	$\frac{\omega}{\omega_{ce0}}\frac{k_r c}{\omega_{ce0}}$	$\int_0^1 \frac{k_i c}{\omega_{ce0}}\frac{dz}{L}$
5	15.26	0.6998	1.623	0.7267	1.093	0.076
10	11.83	0.5769	1.316	0.5964	1.197	0.073
15	9.63	0.4840	1.093	0.5150	1.3125	0.070
20	7.972	0.4095	0.9357	0.4487	1.4325	0.067
25	6.698	0.3484	0.8109	0.3942	1.572	0.064
30	5.724	0.2977	0.7097	0.3485	1.717	
35	4.988	0.2562	0.6280	0.3106	1.870	
40	4.426	0.2220	0.5617	0.2787	2.031	

not provide any indication of the maximum output power or, equivalently, the saturation value of the input power. These must be obtained from quasilinear or nonlinear models of the energy transformation process.

It is, in fact, most striking that the gain decreases only very slowly with increasing beta; one would expect that the maximum output power would be proportional to beta. As we remarked earlier, the fact that the spatial growth rate decreases with beta is in part attributable to the somewhat arbitrary assumption of fixed Δ. Beta is then proportional to the average energy of the hot electrons, and relativistic effects reduce the growth rates. Perhaps more important to the weak beta dependence of the gain is the fact that at low beta the C/A boundary permits very high anisotropy. High anisotropy, in turn, leads to very large spatial growth rates near the midplane. Although lower anisotropy does lead to less peaking of the density near the midplane, the growth is greatly reduced away from the midplane by the increased local magnetic field strength: ω/ω_{ce} is too small to permit large local growth rates.

V. CONCLUSIONS

In Sec. IV we demonstrated that the amplification of an externally launched whistler wave can exceed 40 dB over a relatively wide range of values of beta, $5\% < \beta_\perp \leqslant 25\%$, for typical ECH plasma parameters: $\omega_{pe}^2/\omega_{ce}^2 = 1$, $\Delta = n_h/n = 0.3$, and $1.1 \leqslant \bar{\gamma} \leqslant 1.6$. The corresponding limiting values of temperature anisotropy were $15 \geqslant \eta_{\ell/A} > 6$. These values of anisotropy are much larger than expected in a typical ECH plasma confined in a 2:1 magnetic mirror. Dandl[4] has proposed the use of adiabatic compression to increase η to the C/A boundary value. We have not attempted to include adiabatic compression in the present studies. The gain calculation included the strong spatial variation in hot-electron density and anisotropy, together with the spatial variation in the underlying 2:1 magnetic-mirror field. We conclude from these findings that strong amplification is possible for representative hot-electron equilibria in the linear regime; i.e., for input signals below some power level at which quasilinear or nonlinear effects will saturate the growth of the whistler wave. Clearly the linear theory cannot provide an estimate of this critical parameter; some type of quasilinear calculation of the saturation of whistler growth is required to address this issue.

Existing quasilinear studies of unstable whistler waves in infinite homogeneous plasmas have indicated that, within that highly idealized model, roughly 10% of the hot-electron energy can be transformed into wave energy before the growth rate is reduced to zero. If these estimates provide a valid indication for finite, inhomogeneous, mirror-confined plasmas, it would appear entirely feasible, by operating at higher values of beta in high field strength magnetic fields to achieve very high output power levels. In fact, it may well be that the infinite homogeneous quasilinear model provides an underestimate of the saturation power, since resonant electrons can escape a real magnetic mirror after giving a substantial fraction of their perpendicular kinetic energy to the wave. In effect, a nearly constant level of anisotropy is automatically maintained in an actual magnetic mirror, whereas the infinite, homogeneous quasilinear model allows the anisotropy to decrease as a result of the wave growth.

ACKNOWLEDGMENT

This research was supported by the U.S. Air Force Office of Scientific Research under Contract No. F49620-86-C-0055.

[1] R. N. Sudan, Phys. Fluids **6**, 57 (1963); R. Z. Sagdeev and V. D. Shafranov, Sov. Phys. JETP **12**, 130 (1961); N. T. Gladd, Phys. Fluids **26**, 974 (1983), and references cited therein.

[2] See, for example, H. Ikegami, H. Ikezi, M. Hosokawa, K. Takayama, and S. Tanaka, Phys. Fluids **11**, 1061 (1968); H. J. Booske, W. D. Getty, R. M. Gilgenbach, and R. H. Jong, *ibid.* **28**, 3166 (1985); and references cited in these two works.

[3] C. F. Kennel and H. E. Petschek, J. Geophys. Res. **71**, 1 (1966); see P. A. Bespalov and V. Yu. Trakhtengerts, in *Reviews of Plasma Physics*, edited by M. A. Leontovich (Consultants Bureau, New York, 1986), Vol. 10, p. 155, for an excellent review and substantial bibliography of the Soviet literature.

[4] R. R. Dandl, U.S. Patent No. 4 733 122 (22 March 1988).

[5] A. V. Gaponov-Grekhov, V. M. Glagolev, and V. Yu. Trakhtengerts, Sov. Phys. JETP **53**, 1146 (1982).

[6] See, for example, R. J. Briggs, *Electron Stream Interaction With Plasmas* (MIT Press, Cambridge, MA, 1963).

[7] See, for example, G. E. Guest and D. J. Sigmar, Nucl. Fusion **11**, 151 (1971).

[8] G. E. Guest and R. R. Dory, Phys. Fluids **8**, 1853 (1965).

[9] G. E. Guest and R. L. Miller, Nucl. Fusion **28**, 419 (1988).

[10] H. Grad, Phys. Fluids **9**, 225 (1966).

[11] A. H. Iiyoshi, H. Yamato, and S. Yoshikawa, Phys. Fluids **10**, 749 (1967).

4. RECENT RESULTS

In this section we summarize the most recent results achieved, including a preliminary estimate of the maximum fraction of the plasma energy that can be transformed into RF energy, and a brief discussion of the propagation characteristics of whistlers in candidate PEMS devices. Work in both of these areas was undertaken in anticipation of intensive research into the non-linear limits on the PEMS concept and the geometrical optics issues that must be resolved to ensure efficient coupling of the output microwave fields.

THERMODYNAMIC ESTIMATES OF THE MAXIMUM FRACTION OF THE HOT-ELECTRON ENERGY THAT CAN BE TRANSFORMED INTO MICROWAVES

Thermodynamic techniques developed by C. S Gardner [6], T. K. Fowler [5] and others can be used to estimate the maximum fraction of the mirror-confined hot-electron kinetic energy that can be transformed into microwaves. Here we recapitulate the essential elements of the thermodynamic approach and apply it to the PEMS concept.

The microwave energy within some volume V is given by

$$F = \int_V d^3x \; (\varepsilon_0 E^2/2 + B^2/2\mu_0)$$

$$= \int_V d^3x \; \varepsilon_0 E^2$$

Following Fowler [5] we define a free energy for the anisotropic,

hot-electron plasma:

$$A \equiv 1/2 \int_V d^3x \int d^3v \; \{G(f) - G(g) + mv^2(f - g)/2\} + F$$

where

$$G(h) \equiv h \ln (h/C) - h$$

and the reference distribution function, g, is given by

$$g \equiv C \exp\left(\frac{-mv^2}{2T}\right),$$

corresponding to thermal equilibrium. The parameters C and T are chosen to minimize the value of A(0) at an initial time when the microwave energy is negligible. It can be shown [ ] that A(0) is an upper bound on F; and in particular, if the equilibrium hot-electron distribution function f is the $\ell = 0$ bi-Maxwellian case assumed in most of the studies reported here,

$$F \leqslant \frac{nT_\perp}{4} V \left(\frac{T_\perp - T_\parallel}{T_\perp}\right)^2.$$

Thus, averaged over the plasma volume V,

$$F/V = \varepsilon_0 E^2 \leqslant \frac{nT_\perp}{4} \left(1 - \frac{1}{y}\right)^2.$$

The total kinetic energy stored in the mirror-confined hot electron is given for this distribution function by

$$W = nT_\perp \left(1 + \frac{1}{2y}\right).$$

Thus, the maximum fraction of the total hot-electron kinetic energy that can be transformed into microwave energy is given by

$$\frac{\varepsilon_o E^2}{W} \leq \frac{1}{4y} \frac{(y-1)^2}{(y+0.5)}.$$

In the limit $y \rightarrow \infty$, this fraction approaches 25%; the limit is 20% for $y = 11.6$ and 10% for $y = 3.1$. Thus, over the range of values of temperature anisotropy examined in this report, 10 - 20% of the hot-electron energy is expected to be transformed into microwave energy in an individual microwave pulse. It is important to recognize that the energy remaining in the hot-electron plasma is not lost, and can be utilized in succeeding pulses. In fact, the repetition rate of the pulses can be much greater than the inverse of the initial buildup time of the hot-electron plasma precisely because of the energy remaining after each pulse; it is only the energy transformed into microwave power that must be replaced. The average conversion efficiency can therefore be very high, provided the rate of energy replacement (by UORH) exceeds the rate at which hot electrons are lost from the magnetic mirror by Coulomb scattering into the loss cone. These losses can be very small; the dominant power drain is likely to be that which is associated with the continuous throughput of low-temperature plasma. This power is supplied through fundamental ECH.

GEOMETRICAL OPTICS OF WHISTLER WAVES IN CANDIDATE PEMS GEOMETRIES

We have carried out a preliminary study of the propagation properties of whistler waves launched at one end of a PEMS device and extracted from the opposite end. Since the wave propagation is governed mainly by the colder plasma component, we can obtain a preliminary view of the wave characteristics by making two plausible assumptions regarding the variation of cold-plasma density along the magnetic lines of force. These are

1. within the magnetic mirror region the cold-plasma pressure and temperature are constant; and
2. in the region outside the magnetic mirror, the plasma flows along the diverging magnetic field lines, and local ionization is negligible.

The first assumption implies that the dimensionless ratio of electron plasma and gyrofrequencies, ω_{pe}/ω_{ce}, varies inversely with magnetic intensity, B:

$$\omega_{pe}/\omega_{ce} \propto B^{-1}.$$

The second assumption leads us to expect the exterior cold-plasma density to vary as B^4; since

$$n \sim \frac{N}{\text{Vol.}} \sim \frac{N}{B^{-4}} \sim B^4 \quad \text{for constant N.}$$

We apply this approach to the AMPHED magnetic field operated in its flat-field configuration.

5. CUMULATIVE CHRONOLOGICAL LIST OF WRITTEN PUBLICATIONS

1. G. E. Guest and R. L. Miller, "Formation of Stable, High-Beta, Relativistic-Electron Plasma Using Electron Cyclotron Heating", Nuclear Fusion 28, 419 (1988).

2. G. E. Guest and R. L. Miller, "Amplification of Whistler Waves Propagating Through Inhomogeneous, Anisotropic, Mirror-Confined Hot-Electron Plasmas", Phys. Fluids 31, 3690 (1988).

6. PERSONNEL INVOLVED

G. E. Guest, R. A. Dandl, and R. L. Miller.

7. COUPLINGS

1. Papers presented at conferences:

   "The Plasma Electron Microwave Source (PEMS) Concept: A Novel Approach to Generating Intense Pulses of Microwave Power", G. E. Guest and R. A. Dandl, 1988, IEEE International Conference on Plasma Science, 6-8 June 1988.

   "A Comparison of One- and Two-Dimensional Fokker-Planck Models of Electron Cyclotron Heating", by G. E. Guest and R. L. Miller; 29th Annual Meeting of the Division of Plasma Physics of the American Physical Society, 2-6 November 1987.

   "Generation of Relativistic-Electron Plasmas using Electron Cyclotron Heating: Theory of ECH Runaway", by G. E. Guest, R. L. Miller and C. S. Chang, 28th Annual Meeting of the Division of Plasma Physics of the American Physical Society, 3-7 November 1986.

2. Consultive/Advisory Functions:

   Technical Consultation, 24 February 1987, Air Force Geophysics Laboratory, Hanscomb Air Force Base including a formal presentation, "Properties and Applications of Hot-Electron Plasmas Formed by Electron Cyclotron Heating"

Technical Presentation, 15 October 1987, at a Program Review of Plasma Defense Technology, Los Angeles, California including a formal presentation, "Laboratory Simulation of the Alfven Maser Concept".

Technical Consultation, 26 February 1988, Air Force Weapons Laboratory at Kirtland Air Force Base including a formal presentation, "The Theory of Wave Generation of ECH Plasmas. . . the PEMS Concept for High-Power Microwave Sources".

REFERENCES

1. Raphael A. Dandl, "Method and Apparatus for Producing Microwave Radiation", U.S. Patent No. 4,733,133, March 22, 1988.

2. R.A. Dandl, H.O. Eason, P.H. Edmonds, and A.C. England, Nucl. Fusion 11, 411 (1971).

3. G.E. Guest and R.L. Miller, Nucl. Fusion 28, 419 (1988).

4. G.E. Guest and R.L. Miller, Phys. Fluids 31, 3690 (1988).

5. T.K. Fowler, Phys. Fluids 7, 249 (1964); and Phys. Fluids 8, 459 (1965).

6. C.S. Gardner, Phys. Fluids 6, 839 (1963).